Journal of Molecular Structure 1123 (2016) 284–299

Contents lists available at ScienceDirect

Journal of Molecular Structure

journal homepage: http://www.elsevier.com/locate/molstruc

Spectral investigations of 2,5-difluoroaniline by using mass, electronic absorption, NMR, and vibrational spectra

Etem Kose [a, *], Mehmet Karabacak [b], Fehmi Bardak [a], Ahmet Atac [a]

[a] Department of Physics, Celal Bayar University, Manisa, Turkey
[b] Department of Mechatronics Engineering, H.F.T. Technology Faculty, Celal Bayar University, Turgutlu, Manisa, Turkey

ARTICLE INFO

Article history:
Received 3 May 2015
Received in revised form
25 May 2016
Accepted 26 May 2016
Available online 27 May 2016

Keywords:
2,5-difluoroaniline
DFT
Mass spectrum, FT-IR and FT-Raman spectra
NMR and UV spectra
ESP and DOS

ABSTRACT

One of the most significant aromatic amines is aniline, a primary aromatic amine replacing one hydrogen atom of a benzene molecule with an amino group (NH_2). This study reports experimental and theoretical investigation of 2,5-difluoroaniline molecule (2,5-DFA) by using mass, ultraviolet–visible (UV–vis), ^1H and ^{13}C nuclear magnetic resonance (NMR), Fourier transform infrared and Raman (FT-IR and FT-Raman) spectra, and supported with theoretical calculations. Mass spectrum (MS) of 2,5-DFA is presented with their stabilities. The UV–vis spectra of the molecule are recorded in the range of 190–400 nm in water and ethanol solvents. The ^1H and ^{13}C NMR chemical shifts are recorded in $CDCl_3$ solution. The vibrational spectra are recorded in the region 4000–400 cm^{-1} (FT-IR) and 4000–10 cm^{-1} (FT-Raman), respectively. Theoretical studies are underpinned the experimental results as described below; 2,5-DFA molecule is optimized by using B3LYP/6-311++G(d,p) basis set. The mass spectrum is evaluated and possible fragmentations are proposed based on the stable structure. The electronic properties, such as excitation energies, oscillator strengths, wavelengths, frontier molecular orbitals (FMO), HOMO and LUMO energies, are determined by time-dependent density functional theory (TD-DFT). The electrostatic potential surface (ESPs), density of state (DOS) diagrams are also prepared and evaluated. In addition to these, reduced density gradient (RDG) analysis is performed, and thermodynamic features are carried out theoretically. The NMR spectra (^1H and ^{13}C) are calculated by using the gauge-invariant atomic orbital (GIAO) method. The vibrational spectra of 2,5-DFA molecule are obtained by using DFT/B3LYP method with 6-311++G(d,p) basis set. Fundamental vibrations are assigned based on the potential energy distribution (PED) of the vibrational modes. The nonlinear optical properties (NLO) are also investigated. The theoretical and experimental results give a detailed description of the structural and physicochemical properties of the title molecule and contribute to understanding of the nature of di-substituted aniline derivatives.

1. Introduction

Aniline is one of the most significant aromatic amines, a primary aromatic amine replacing one hydrogen atom of a benzene molecule with an amino group. Aniline and its derivatives use industrial and commercial applications, dyestuff, pesticide, and pharmaceutical manufacturing, photographic chemicals resins [1,2]. Even though these compounds are considered to be environmentally toxic pollutants, they serve as precursors in the production of several drugs, such as analgesics, central nervous depressants, and antibiotics [3,4]. Fluoroanilines (FA) are significant due to their exciting biological activities like being key intermediates in the manufacture of agrochemicals (pesticides, herbicides, and fungicides) [5]. The other interesting usage of fluoroaniline polymers as precursors in the synthesis of glucose biosensors and modifiers of electrodes in bacterial fuel cells has been published [6,7].

There have been various spectroscopic studies containing aniline and its derivatives, due to their exciting features and chemical importance. Some of these are listed below in historical order; the Raman spectrum of aniline were recorded in 1942 [8]. Vibrational assignment based FT-IR and Raman spectra have already been reported for aniline [9]. The far-infrared vapor phase spectra of aniline-ND_2 and aniline-NHD were presented [10]. The vibrational spectrum of aniline was explored on the basis of normal coordinate

* Corresponding author.
E-mail address: etemmm43@gmail.com (E. Kose).

http://dx.doi.org/10.1016/j.molstruc.2016.05.088
0022-2860/

analysis [11]. An interesting study of the structural as well as the electronic properties of aniline was reported by using several DFT-based methods [12]. The structural studies of aniline are reported by various scientists; experimental papers were presented (in the gas phase) by microwave spectroscopy [13,14], electron diffraction [15], X-ray crystallography [16], theoretically using semi-empirical [17,18], ab initio methods [18–21] and using several quantum computational methods [22].

The other studies on some fluorinated derivatives of aniline, in our interest, are gathered as follows: infrared spectra of anilines fluorinated derivatives were presented with some tentative assignments [23,24]. Infrared spectrum of 2,3-fluoroaniline was recorded and the vibrational assignments were made for the observed fundamental frequencies [25]. The far infrared spectra of aniline (gas phase) and 4-fluoroaniline [26], and vibrational Raman spectrum and the calculations of para-fluoroaniline [27] have been reported. The N–H stretching frequencies of aniline, 2FA, 3FA, and 4FA (gas phase) were studied by using the IR-UV double resonance spectroscopy by Honda et al. [28]. Theoretical Raman and infrared spectra of para-halogen anilines were reported, and corresponding vibrational assignments were given [29]. The IR and Raman spectra, and computational studies of tri-fluoroanilines (2,3,4-, 2,3,6- and 2,4,5-, 2,4,6-FA) by using the HF and B3LYP methods were investigated by Mukherjee and coworkers [30,31]. Recently, the conformational isomers, structural, thermodynamic and electronic properties, chemical shifts, and harmonic vibrational frequencies of 3-methoxyaniline were studied [32]. The observed spectral data (FT-TR, FT-Raman, UV and NMR) of 3,5-difluoroaniline molecule were compared with theoretical values obtained in DFT/B3LYP method [33]. Structural, spectroscopic studies, NBO, NLO analysis and reactivity descriptors of 2,3 and 2,4-difluoroaniline was added in the literature by Pathak et al. [34]. Electrical and structural properties of mono-, di-, tri-, tetra-, and penta-fluoroanilines were investigated using hybrid density functional theory based methods by Shirani and Beigi [35]. The vibronic and cation spectra of 2,5-difluoroaniline were reported Huang et al. [36].

Fluorine is the most electronegative element in the periodic table and has low polarizability. Also, due to polar bonds like δ^{+}C–F δ^{-}, it has a relatively ionic character. So organofluorine compounds show entirely a wide variety of characteristics upon the chemical and physical properties, which are not seen for the other halogens [30,37]. Therefore, the structural and spectroscopic investigations on substituted aniline molecules are accomplished so far. Likewise, fluorinated compounds take part in these types of studies and show of considerable importance.

In this paper, the spectroscopic and structural properties of 2,5-DFA molecule are investigated to provide insight into understanding of physicochemical features of the substance. We concerned on the mass (MS), UV–Vis, ^{13}C and ^{1}H NMR, FT-IR and FT-Raman spectra, combined theoretically by DFT (B3LYP)/6-311++G(d,p) basis set calculations in investigation of the present molecule. The possible fragments are predicted in the mass spectrum. The electronic characteristic details are analyzed based on UV–Vis spectra, DOS, ESPs, Mulliken atomic charges. The possible noncovalent interactions were visualized in RDG analysis. Furthermore, the NLO characteristics and thermodynamic properties were outlined.

2. Experimental details

2,5-DFA molecule was purchased from Across Organics Company in liquid phase with a stated purity of greater than 97% and used with no further purification. The experimental mass spectrum of the title molecule is taken from Spectral Database for Organic Compounds, SDBS [38]. The UV–Vis spectrum of the title molecule dissolved in ethanol and water were taken in the range of 190–400 nm using Shimadzu UV-2101 PC, UV–VIS recording Spectrometer. The ^{1}H and ^{13}C NMR spectra of 2,5-DFA molecule (in $CDCl_3$) were recorded in Varian Infinity Plus spectrometer at 300 K. The chemical shifts were reported in ppm relative to tetramethylsilane (TMS). Lastly, the experimental FT-IR and FT-Raman spectra of the molecule were recorded in the region 4000-400 cm^{-1} and 4000–10 cm^{-1}, respectively, Perkin-Elmer FT-IR System Spectrum BX spectrometer (at room temperature), with a scanning speed of 10 cm^{-1} min^{-1} and the spectral resolution of 4.0 cm^{-1} and Bruker RFS 100/S FT-Raman instrument using (1064 nm excitation from an Nd:YAG laser). The detector is a liquid nitrogen cooled Ge detector, five hundred scans were accumulated at 4 cm^{-1} resolution using a laser power of 100 mW used for FT-IR and FT-Raman spectra.

3. Theoretical information of studies

The DFT [39] method (with the Becke's three-parameter hybrid functional (B3) [40,41] for the exchange part and the Lee-Yang-Parr (LYP) correlation function [42]), has been accepted as a cost-effective approach and favorite one due to its great accuracy in reproducing the experimental values of molecular geometry, atomic charges, dipole moment, thermodynamic properties, vibrational frequencies etc. Gaussian 09 suite of quantum chemical codes are used for all calculations performed [43].

The paper includes following theoretical details; in the first instance, the molecule was optimized to find more stable structure and scan coordinate, selected torsion angle (for NH_2 group of position), which is changed every 10° and molecular energy profile is calculated from 0° to 360°. The results used to calculate the spectroscopic features of the title molecule such as; electronic properties, isotropic chemical shift and vibrational frequencies by using B3LYP with 6-311++G (d,p) basis set calculations.

The TD-DFT method with B3LYP/6-311++G (d,p) basis set is employed to obtain UV–Vis spectrum, electronic transitions, vertical excitation energies, absorbance, and oscillator strengths of the studied molecule. The frontier molecular orbitals (FMOs), such as HOMO and LUMO, energies are obtained also by TD-DFT approach. The density of states, such as TDOS, PDOS and OPDOS of the headline molecule are graphed by using GaussSum 2.2 program [44]. Besides of these calculations, ESPs of 2,5-DFA molecule is given as 2D and 3D size. The thermodynamic properties of 2,5-DFA molecule such that heat capacity, entropy, and enthalpy (from 100 to 700 K) were reported directly from the results of frequency calculations. The RDG of the title molecule is given in graph by using Multiwfn [45] and showed the interactions by using VMD program [46].

The GIAO method is one of the most common approach to have nuclear magnetic shielding tensors and efficient for reliable studies of magnetic properties. Therefore, ^{1}H and ^{13}C NMR isotropic chemical shifts are performed with the GIAO method [47–49] as addressed on optimized parameters with B3LYP/6-311++G (d,p) method.

The vibrational frequencies are not suitable to use directly, due to offset the systematic errors caused by basis set incompleteness, neglect of electron correlation and vibrational anharmonicity [50,51]. Because of these reasons, the scaling factors are employed as 0.983 up to 1700 cm^{-1} and 0.958 for greater than 1700 cm^{-1} [52,53]. The assignments of the fundamental vibrational modes are assigned based on PEDs by using VEDA program [54], and taking extra help for the visual animation and verification of the normal modes are fallen back on by using Gaussview program [55]. NLO properties (the dipole moment, mean polarizability and first static hyperpolarizability) of 2,5-DFA molecule is achieved on the results

of DFT method.

4. Results and discussion

2,5-DFA molecule have three substituents; first one NH_2 group, and two F (fluorine) atoms. We determined an imaginary frequency (3707.57i cm^{-1}) corresponding to NH_2 wagging for the title molecule in the C_S point group symmetry. The title molecule is unstable in C_S point group symmetry due to the imaginary frequency. However, the title molecule has positive frequencies in the C_1 point group symmetry. Therefore, the calculations were recorded according to the C_1 point group symmetry of the title molecule (see Table S1).

4.1. Potential energy surface (PES) scan

To obtain the most stable structure of the present molecule, the conformational flexibility of 2,5-DFA molecule is studied with selected torsion angle of $\tau(H_{12}–N_{10}–C_1–C_6)$ by using B3LYP/6-311++G(d,p) method. This angle was changed in every 10° from 0° to 360°, thus analysis were performed by using scanning between phenyl ring and NH_2 group. The results of conformational analyze for the molecule given in Fig. S1 show that there are four local minima near 30°, 160°, 200° and 330°. The structures (I, II, III, and IV) at each local minimum were re-optimized and the energies were determined as −305110.177516, −305110.177707, −305110.177708, and −305110.177513 kcal/mol, respectively. In terms of energy consideration, these local minimums can be associated to two conformations; conformation A with average energy of −305110.17751 kcal/mol (the structures I and IV), and the conformation B with that of −305110.17771 kcal/mol (the structure II and III). From the structural perspective, the structure I and structure II seems to be the same, however, the dihedral angle of amino group from the molecular plane differs slightly. The orientation of amino group in structure I and structure IV at opposite sides, but the energies are the same. To ensure whether proposed conformations A and B should be taken as two distinct stable structures, the vibrational spectra were also compared. None of the vibrational frequencies show any difference within less than one wavenumber, thus the structure with the lowest energy is accepted as a single and the most possible conformer. Therefore, geometrical structural analyze, vibrational frequencies, NMR chemical shifts, UV–Vis absorption spectra, and other calculations of the present molecule are depicted based on the structure III.

4.2. Geometrical structures

The investigated molecule has NH_2 (amino) group that affects the planarity of the molecule thus making the symmetry in C_1 point group. The energies and some thermodynamical properties are presented for C_1 and C_S point group symmetry of the title molecule in Table S1. The energies are also showed that C_1 point group symmetry is more stable than C_S point group symmetry. Two sets of X-ray data for aniline from Ref. [16] are used to compare the optimized structure parameters of 2,5-DFA molecule, calculated at density functional B3LYP method with 6-311++G(d,p) basis set, because no crystallography data of the present molecule has not been determined. The optimized geometric structures of 2,5-DFA molecule is schemed in Fig. 1 with the atomic symbols and labels. The optimized geometric parameters (bond lengths and angles) are collected in Table 1 based on labeling in Fig. 1.

Table 1 shows the comparison of the experimental values of aniline and optimized geometric parameters of 2,5-DFA molecule. The C–C bonds lengths of 2,5-DFA are displayed disparity from experimental data [16]. The discrepancies can be due to presence of fluorine atoms. If the effect of F atoms taken into account, it seems that the C–C bonds are very good concinnity with the experimental results of aniline [16] molecule (see Table 1). The bond lengths of C–C are obtained theoretically in the range from 1.379 to 1.402 Å. These value are predicted to be from 1.385 to 1.403 Å, 1.382 to 1.401 Å for 2,3-, and 2,4-DFA molecules, respectively [34]. So we can say that the optimized geometric parameters (B3LYP/6-311++G(d,p) method) which are in good coherent with experimental values as in the range of 1.367–1.404 Å and 1.364–1.407 Å for aniline [16]. Considering all theoretical results, the correlations of C–C bonds lengths well agrees with the literature for the structurally similar molecules [29–34,56–58].

The C–NH_2 bond length is calculated as 1.386 Å for 2,5-DFA molecule. Theoretical result of C–N corresponds to the same region with experimental value of 1.398 and 1.386 Å for aniline [16]. In the literature; the C–NH_2 bond lengths were calculated as 1.389 and 1.388 Å for 2,4,5-TFA (tri-fluoroaniline) and 2,4,6-TFA, respectively [59]. Pathak et al. reported these bonds at 1.389 Å for 3,5-DFA [33] and 1.388 and 1.394 Å for 2,3- and 2,4-DFA [34] molecules, respectively.

The optimized N–H_2 (amino group) bond lengths are obtained at ca. 1.008 Å by B3LYP with 6-311++G(d,p) method. Some small differences can be seen by comparing these values with experimental value of 1.070 and 0.940 Å (structure I of ref. [16]), and 0.990 and 0.770 Å (structure II of ref. [16]). The N–H bonds lengths are computed nearly equal as compared to the initial values for aniline, which infers that the N–H bonds are not sensitive regarding to the presence of F atom(s) in the ring. Similar observations has also been published in literature [29–34,56–58].

By the substitution of halogens (F, Cl, Br …) in place of hydrogen atoms, remarkable increments are expected in the bond lengths. The C–F bond lengths are predicted at 1.365 Å (for C–F13) and 1.357 Å (for C–F14) for 2,5-DFA molecule, by using B3LYP/6-311G++(d,p) basis set. The bonds before replacement of fluorine atoms were observed as ca. 1.05 Å for the structure of aniline [16]. We can say the C–F bond lengths are different for the title molecule. The differences can be caused from the location of F atoms in the molecule. As seen in similar molecules; C–F bond lengths were obtained at 1.354 Å for 3,5-DFA molecule [33], recorded at 1.361, 1.352 and 1.356 Å for monofluoroaniline (2-, 3- and, 4-) isomers [60], determined at 1.354 ± 0.006 Å for fluorobenzene by microwave spectroscopy [61]. These bonds were also computed at 1.356 Å, 1.362 Å for 2,3-DFA, and 1.348 Å, 1.358 Å for 2,4-DFA molecules, respectively [34]. Mukherjee et al. predicted C–F bonds at 1.348 Å for 2,4,5-TFA and 1.354 Å for 2,4,6-TFA and 1.366 Å for 4FA [59] and observed as 1.363 Å in 4FA [62]. There are even more literature reports very similar results to outcomes of our results [29–34,53–55,63].

Some irregularity are seen in ring angles both endohedral and exohedral. The dihedral angles are carried out (C2–C1–N10–H12) as −19.2° and (C6–C1–N10–H11) as 25.4° for 2,5-DFA molecule. The substitution on the aniline ring has been found to change this angle and also affects the degree of pyramidalisation by resonance effects than inductive effects [64,65]. The nitrogen is pyramidal with the dihedral angle between the plane of the aromatic ring and the NH_2 plane being 37.5° [65]. This dihedral angle between the NH_2 plane and the plane of the aromatic ring was found as −22.4° and 22.4° [33]. The dihedral angles (C–C–N–H) were obtained at −19.7°, −20.4° for 2,3-DFA, and 25.4°, 28.4° and for 2,4-DFA molecule [34]. In this study, the dihedral angles are computed as −19.2° and 25.4° showing good correlation with related molecules reported above [57,64–66].

The substitution F atoms attached C2, C5 carbon atoms and NH_2 group attached C1, leads to some changes of the bond lengths and angles in normal phenyl ring. As the discussion of the paper [60] for

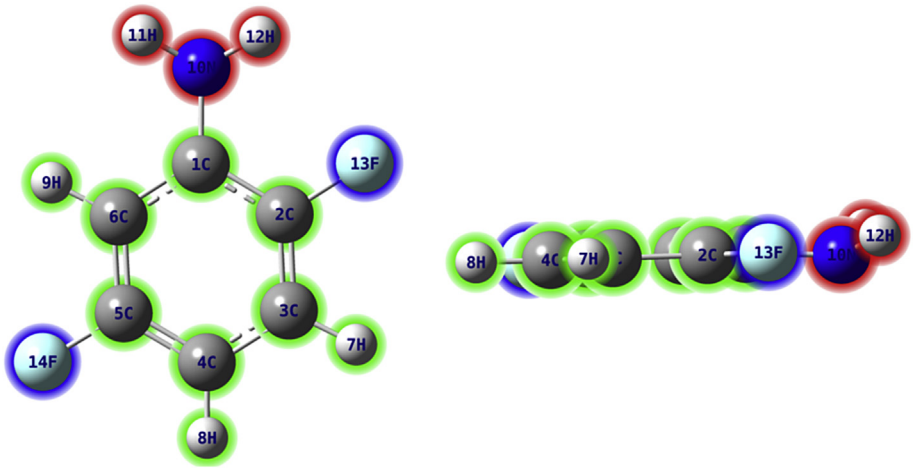

Fig. 1. The optimized geometric structures of 2,5-DFA.

Table 1
The experimental and optimized bond lengths (Å) and angles (°) for aniline and 2,5-DFA molecules.

Parameters	Aniline X-Ray[a]		B3LYP 6-311++G(d,p)
Bond lengths (Å)			
C_1-C_2	1.404(6)	1.407(6)	1.401
C_1-C_6	1.386(6)	1.385(6)	1.402
C_1-N_{10}	1.398(6)	1.386(6)	1.386
C_2-C_3	1.380(7)	1.389(7)	1.379
C_2-F_{13}	–	–	1.365
C_3-C_4	1.386(7)	1.364(7)	1.396
C_4-C_5	1.391(7)	1.383(7)	1.385
C_5-C_6	1.367(7)	1.379(7)	1.385
C_5-F_{14}	–	–	1.357
$N_{10}-H_{11}$	1.070(5)	0.990(4)	1.008
$N_{10}-H_{12}$	0.940(6)	0.770(6)	1.009
$C\text{-}H_{average}$	1.010	0.952	1.082
Bond angles (°)			
$C_2-C_1-C_6$	117.9(4)	117.9(4)	117.0
$C_2-C_1-N_{10}$	119.9(4)	120.4(4)	120.4
$C_6-C_1-N_{10}$	122.0(4)	121.5(4)	122.5
$C_1-C_2-C_3$	119.7(4)	122.0(4)	123.2
C_1-C_2-H/F_{13}	113.0(2)	115.0(3)	117.1
C_3-C_2-H/F_{13}	128.0(2)	125.0(3)	119.7
$C_2-C_3-C_4$	122.1(5)	121.2(5)	119.6
$C_2-C_3-H_7$	124.0(4)	122.0(2)	119.2
$C_4-C_3-H_7$	118.0(4)	118.0(2)	121.3
$C_3-C_4-C_5$	117.6(5)	119.2(5)	117.6
$C_3-C_4-H_8$	120.0(3)	120.0(3)	121.9
$C_5-C_4-H_8$	123.0(3)	121.0(3)	120.5
$C_4-C_5-C_6$	120.9(5)	120.6(5)	123.3
C_4-C_5-H/F_{14}	115.0(3)	118.0(2)	118.8
C_6-C_5-H/F_{14}	124.0(3)	122.0(2)	117.9
$C_1-C_6-C_5$	121.8(4)	121.1(4)	119.4
$C_1-C_6-H_9$	111.0(3)	128.0(3)	120.9
$C_5-C_6-H_9$	127.0(3)	111.0(3)	119.7
$C_1-N_{10}-H_{11}$	103.0(4)	113.0(4)	116.6
$C_1-N_{10}-H_{12}$	124.0(3)	121.0(2)	115.9
$H_{11}-N_{10}-H_{12}$	119.0(4)	104.0(5)	113.9
Selected dihedral angles[b] (°)			
$C_2-C_1-N_{10}-H_{11}$			−157.4
$C_2-C_1-N_{10}-H_{12}$			−19.2
$C_6-C_1-N_{10}-H_{11}$			25.4
$C_6-C_1-N_{10}-H_{12}$			163.6
$C_6-C_1-C_2-F_{13}$			−179.5
$C_1-C_6-C_5-F_{14}$			−179.9

[a] The X-Ray data from Ref. [16].
[b] A dihedral angle between the NH_2 group or F atoms and the ring plane.

fluoroanilines, the calculated CCC angles in the aromatic ring of fluoroanilines, the structural changes are consistent with the σ electron-withdrawing (inductive) effect of the fluorine substituent at different sites of the ring. As seen, the results (see Table 1) ring C–C–C and C–C–H bonds angles deviated from normal value of 120°.

A brief glimpse; the phenyl ring is found to be slightly deformed from the ideal hexagonal structure due to substitution of NH_2 group and heavy F atom. Therefore, the interaction between the substituents and the ring are affected by the ring geometry. There are small differences between the computed and experimental results [16] of the optimized parameters. Therefore, the substitution of highly electronegative F atoms decreases the electron density at ring and thus corresponding bond length changes. This can be due to the theoretical results belong to vapor phase and the experimental results belong to liquid phase and had aniline molecule.

4.3. Mass spectrum

Mass spectrometry (MS) helps identifying the amount and type of fragments present in a sample. Mass spectrum is generally presented as a vertical bar graph, in which each bar represents an ion having a specific mass-to-charge ratio (m/z) and the length of each bar shows the relative abundance of that ion. Most of the ions formed in a mass spectrometer have a single charge; therefore, the m/z value is equivalent to mass itself. The most intense peak is assigned as the base peak corresponding to the abundance of 100%. Generally, molecular weight peak observed in a spectrum represents the parent molecule lost an electron and is termed as the molecular ion (M+). Small peaks (M+1, M+2, …etc.) are also observed above the calculated molecular weight (molecular ion (M+)) due to the natural isotopic abundance of ^{13}C, ^{2}H, …. etc.

In this paper, mass spectrum of 2,5-DFA was investigated to analyze possible ionic fragmentations and their stabilities. The experimental mass spectrum of the title molecule [38] is given in Fig. 2. The possible fragments were identified by their mass-to-charge ratio (m/z). The mass spectrum of 2,5-DFA displays strong molecular ion peak (M+) (at the same time base peak) at m/z = 129 and main molecule showed in Fig. 3. A single M+1peak with m/z = 130 appears due to isotopic abundance of ^{13}C. The first and smallest stable neutral fragment can be the HF molecule leaving $[C_6H_4FN]^+$ cation fragment (Fig. 3a) behind causing the first nearest peak with m/z = 109 to M+. The peaks at m/z = 102 and m/z = 101 peaks on the spectrum were assigned to $[C_5H_4F_2]^+$ and $[C_5H_3F_2]^+$

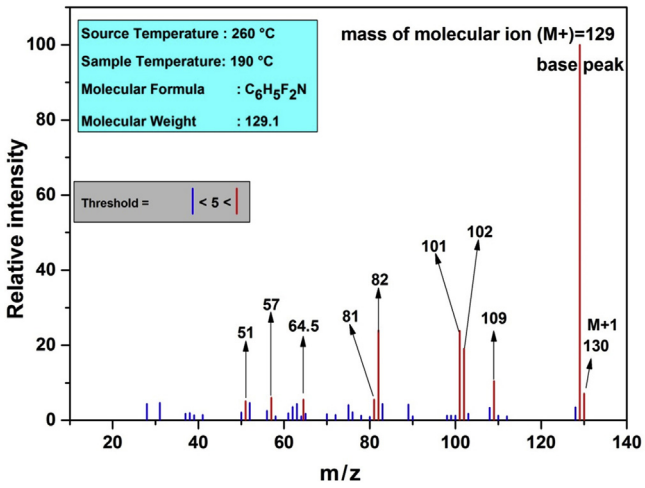

Fig. 2. The mass spectra of 2,5-DFA molecule showing some fragments peaks.

fragments appear in nearly the same intensity. They formed by total breaking of the ring structure. These fragments are $[C_5H_4]^+$ [70], $[C_4H_9]^+$ [71], $[C_4H_3]^+$ [72] (Fig. 3g–i), respectively. Their m/z rates are 64.5, 57 and 51, respectively. The fragmentations are generally supported in the literature [67–72].

4.4. Electronic characteristics details

4.4.1. UV–Vis spectra and molecular orbital investigations

The UV–Vis (electronic absorption) spectra of 2,5-DFA molecule are obtained by experimental and theoretical techniques by using Shimadzu UV-2101 PC, UV–VIS recording Spectrometer and TD–DFT method with B3LYP/6-311++G (d,p) basis set (root = 40), respectively. The experimental results are recorded at room temperature in ethanol and water solutions. TD–DFT method are chosen due to the results are a quite reasonable and computationally more expensive than semi-empirical methods and allow easily studies of medium size molecules [73–75]. The experimental and theoretical UV–Vis (electronic absorption) spectra of the title

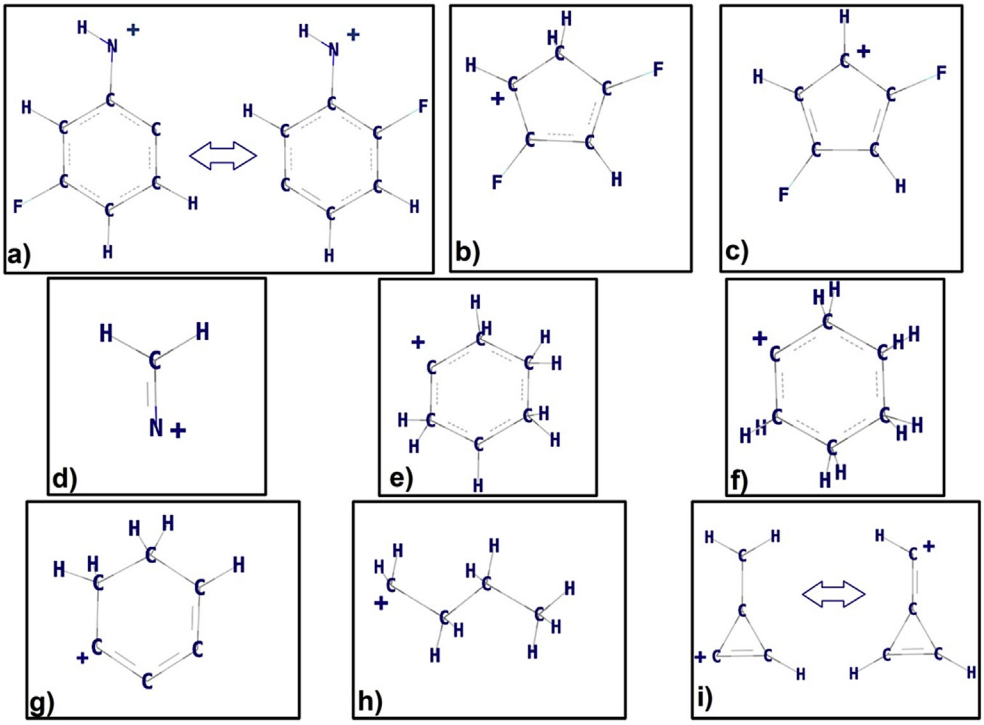

Fig. 3. The possible fragments of 2,5-DFA molecule showing cations.

fragments (Fig. 3b and c.), respectively. Formation of these cations can occur as the breaking of the ring and reformation. During this process, the bond structure and stability changes significantly, too. These two fragmentations occur possibly by H–C≡N and H_2CN^+ groups leaving the parent molecule, respectively. Meanwhile, H_2CN^+ fragment (Fig. 3d) produces a weak peak at m/z = 28 as a result of the same separation processes. The peaks at m/z = 82 and m/z = 81 are identified as $[C_6H_9]^+$ [67] and $[C_6H_{10}]^+$ fragments [68] (Fig. 3e and f). These peaks are characteristics of the mass spectra of benzene derivatives [69]. These suggest cyclohexane type cation formations with the first nearest cation appearing at m/z = 78 for the pure benzene molecule whereas leaving of F atoms from the ring causes faster binding of multiple hydrogens on the carbons giving rise to cations with higher m/z ratios in our case. Three small molecule are shown in Fig. 4. The theoretical and experimental absorption wavelengths (λ), excitation energies (E), oscillator strengths (*f*), and calculated counterparts with major contributions can be seen in Table 2 for the gas phase, ethanol, and water solvents. The calculated values are showed well agree experimental results. We observed three peaks which are 201.54, 233.18, 284.99 nm in ethanol and 193.08, 225.95, 278.74 nm in water. These peaks are calculated at 201.46, 225.08, 261.92 nm in ethanol and 201.70, 225.08, 261.84 nm in water, for 2,5-DFA molecule. All these calculated values are in good agreement with the experimental data.

The highest occupied molecular orbital (HOMO) and the lowest unoccupied molecular orbital (LUMO) as named also primary frontier molecular orbitals (FMOs) are significant for electric and

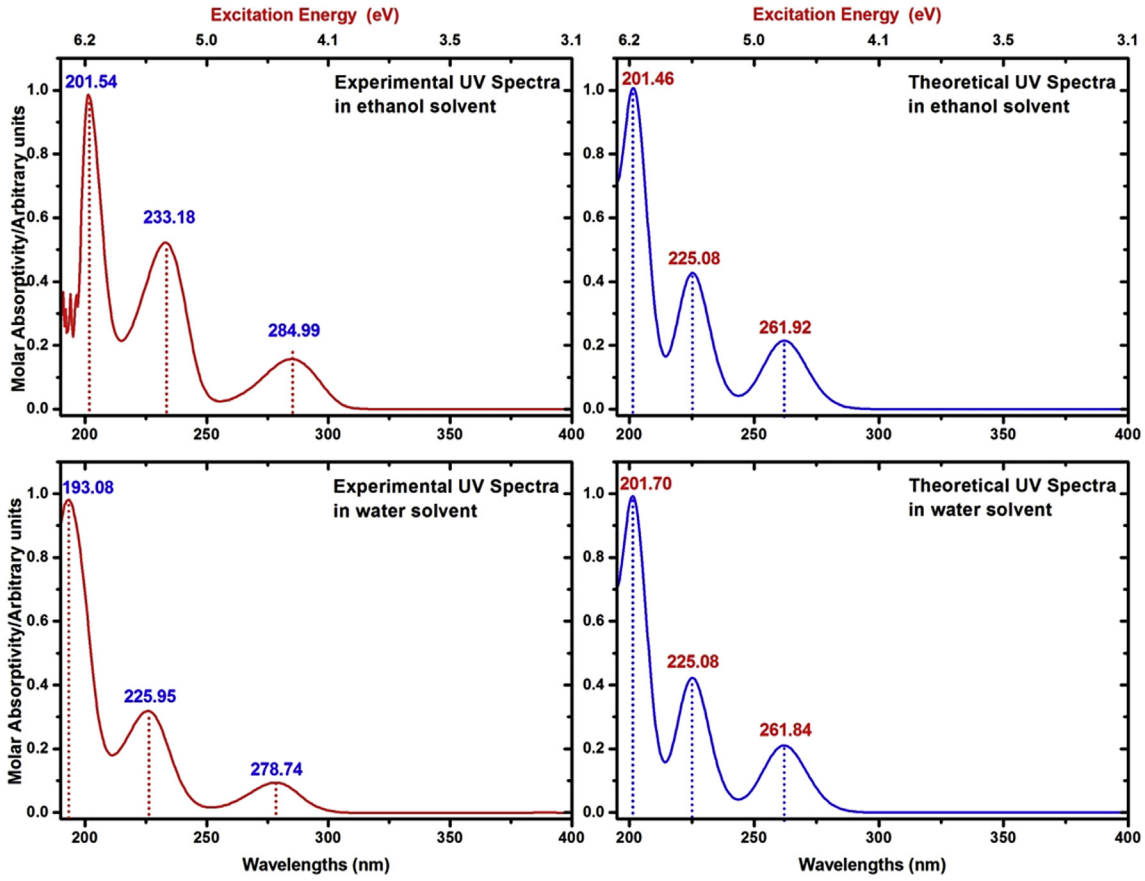

Fig. 4. The experimental and theoretical UV–Vis spectrum of the 2,5-DFA in ethanol and water.

Table 2
Experimental and calculated wavelengths λ (nm), excitation energies (eV), oscillator strengths (*f*) of 2,5-DFA for gas phase, in ethanol and water solutions.

TD-DFT					Experimental	
	f	Major contributes	λ (nm)	E (eV)	λ (nm)	E (eV)
Gas	0.0582	H → L (82%)	260.98	4.7513	–	–
	0.0068	H → L + 1 (96%)	251.14	4.9376	–	–
	0.0548	H → L + 3 (37%), H → L + 2 (37%), H-1 → L (20%)	222.70	5.5680	–	–
	0.0037	H → L + 5 (86%)	202.42	6.1259	–	–
Water	0.0790	H → L (84%)	261.84	4.7356	278.74	4.4486
	0.0049	H → L + 2 (80%), H → L + 1 (17%)	240.68	5.1521	–	–
	0.1562	H → L + 1 (53%), H-1 → L (25%)	225.08	5.5091	225.95	5.4879
	0.3472	H-1 → L (57%), H → L + 1 (15%), H → L + 2 (10%)	201.70	6.1477	193.08	6.4222
Ethanol	0.0807	H → L (85%)	261.92	4.7343	284.99	4.3510
	0.0048	H → L + 2 (53%), H → L + 1 (44%)	241.04	5.1444	–	–
	0.1577	H → L + 1 (34%), H → L + 2 (31%), H-1 → L (25%)	225.08	5.5091	233.18	5.3178
	0.3473	H-1 → L (58%), H → L + 1 (21%)	201.46	6.1551	201.54	6.1526

H:HOMO, L:LUMO.

optical properties. The ability of electron giving and accepting characterizes are showed by the HOMO and LUMO, respectively. The potential energy difference between the HOMO and LUMO are describes energy gap; basically, it is how much energy has to be fed into the molecule to kick it from the ground (most stable) state into an excited state [76]. The surfaces and energy gaps of frontier orbitals (H, L, L+1, L+2, and L+3) are represented in Fig. 5. The frontier orbitals energies and energy gaps are collected in Table S2. The energy gap values of the title molecule are calculated the same value at 5.42 eV for gas phase, ethanol, and water solvents by using TD-DFT/B3LYP/6-311++G(d,p) method. The HOMO and LUMO orbital, have the positive phase is red and the negative one is green-yellow nodes. The charge density of HOMO localized the entire molecule symmetrically. The charge distribution of LUMO is changed on H and F atoms. The important energy gaps values of FMOs of the studied molecule are also given in Table S2. Such as, H−1→L+2, H→L+1, H→L+2 and H→L+3 energy gaps values of the molecule are a critical parameter in determining molecular electrical transport properties. These values are recorded in ethanol and water solvents for the studied molecule gathered in Table S2. The molecular orbital orient of 2,5-DFA molecule to see energy levels and energy gaps are given in Fig. S2.

A chemical hardness, electronegativity, chemical potential and electrophilicity index are obtained by use of HOMO, LUMO energies

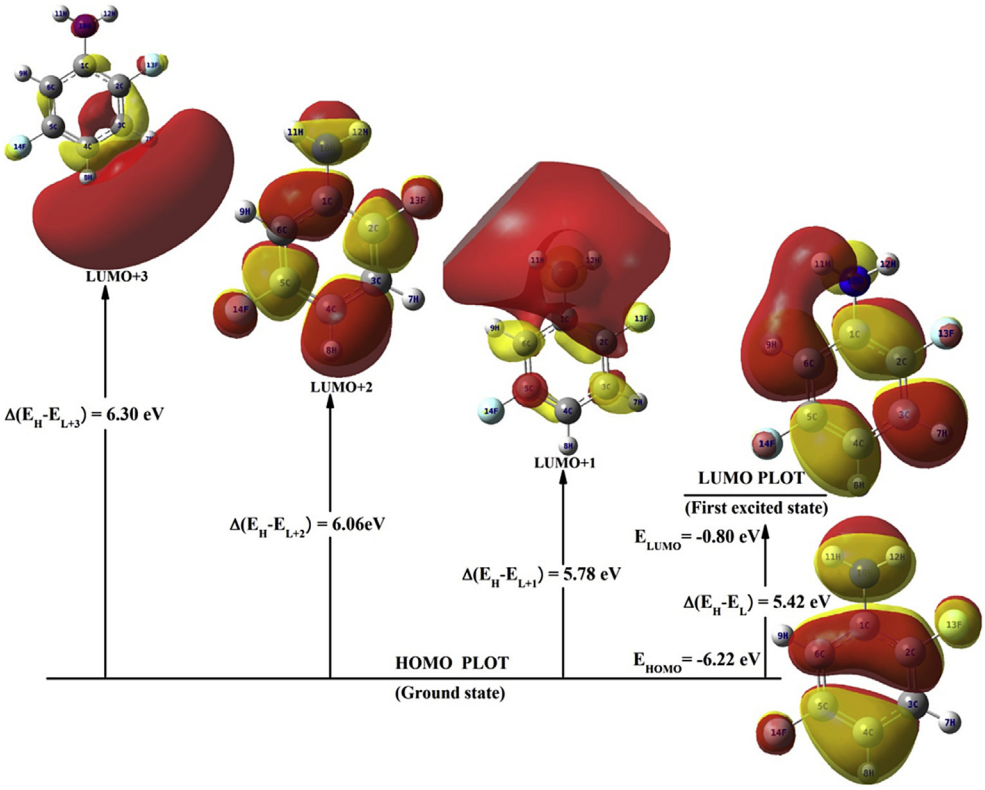

Fig. 5. The selected frontier molecular orbitals of 2,5-DFA with the energy gaps.

for the headline molecule in gas phase, ethanol and water solutions in Table S2. They are good indicators of the chemical stability of molecular systems [76,77]. The chemical hardness (η) and potential (μ), which are an index of reactivity and measures the escaping tendency of electron cloud, respectively, are given by Parr and Pearson [78], η=(I−H)/2 and μ = −(I−H)/2 where I and H are ionization potential and electron affinity of a molecular system [78]. The chemical hardness shows that if the molecule has large energy gap, it is a hard molecule or if the molecule has small energy gap it is a soft molecule. Also hard molecule is less polarizable than the soft molecules because it needs higher excitation energy. Electronegativity (χ) is described as negative of the electronic chemical potential. The global electrophilicity index (ω) has been given by the following expression; $\omega = \mu^2/2\ \eta$ [79]. The chemical hardness (η) values have the same magnitude for ethanol and water solvents. The chemical potential and electrophilicity index decrease in the solvents. This is basically due to intermolecular interactions exist between solute and solvent. During the course of these interactions, the reactive sites of solute molecules are concealed by the solvent molecules; therefore, a decrease in the chemical potential and electrophilicity index is expected.

4.4.2. Total, partial, and overlap population density-of-states

The neighboring orbitals in the boundary region may show quasi-degenerate energy levels. The total density of states (TDOS), partial density of states (PDOS), and overlap population density of states (OPDOS or COOP (Crystal Orbital Overlap Population)) [80–82], are obtained by convoluting the molecular orbital information with Gaussian curves of unit height and Full width at half maximum (FWHM) of 0.3 eV using the GaussSum 2.2 program [44] in point of the Mulliken population analysis.

The TDOS graphs denote the number of states in unit energy interval. In isolated systems, the energy levels are separate, and the concept of DOS is, thus, somewhat questionable. However, if the discrete energy levels are broadened to curves artificially, DOS graph becomes a valuable tool for visually characterizing orbital compositions [83–85]. Due to the HOMO and LUMO may not yield a realistic description of the frontier orbitals. The interaction of two orbitals, atoms or groups described as bonding, anti-bonding and nonbonding. The OPDOS diagrams define bonding character of these groups based on positive, negative and zero value, indicated a bonding, anti-bonding, and nonbonding interactions, respectively [86,87]. Additionally, to determine and compare of the donor–acceptor properties of the ligands is prepared OPDOS diagrams.

The density of states graphics of the studied molecule are listed in Figs. S3–S5, named TDOS, PDOS and OPDOS, respectively. The composition of the fragment orbitals contributing to the molecular orbitals of molecule are employed PDOS graphs. The contribution of phenyl ring, fluorine atoms and NH_2 group are nearly 100% and there is almost no contribution of hydrogen atoms (ring) in HOMO orbitals for 2,5-DFA molecule. A phenyl ring, fluorine atoms and NH_2 group provide different contribution in LUMO orbitals. Phenyl ring (87%) and NH_2 group (13%) contribute 2,5-DFA molecule, respectively. To determine bonding and anti-bonding character of atom or groups is difficult looking percentage sharing of atomic or molecular orbitals in the molecules. Therefore, the OPDOS diagrams easily showed that interaction or no interaction between selected atoms or groups based on energy values of its orbitals. Such as fluorine atoms ↔ NH_2 group (blue line) system is positive (anti-bonding interaction) as well as phenyl ring ↔ NH_2 group systems (red line). Ring ↔ fluorine atom (black line) is negative (bonding interaction) in HOMO orbitals of molecules. The OPDOS plots of the studied molecule showed that bonding character in LUMO.

4.4.3. Electrostatic potential surface

The molecular electrostatic potential (MEP) or electrostatic potential (ESP) surfaces are related to electronic density and useful to define sites for electrophilic attack and nucleophilic reactions as well as hydrogen bonding. These surfaces of molecules are mainly allow to know the reactive behavior of the molecules, in that the positive regions are electrophilic centers whereas, negative regions can be regarded as potential nucleophilic sites, indicated as blue and red color, respectively [76,88–90]. The 2D contour and 3D (two and three dimensional) diagrams of ESPs are illustrated in Fig. 6. The electrostatic potential at the surface values increase in the order red to blue ranging from −5.115 e-2 to 5.115 e-2 (a.u.) for 2,5-DFA molecule. The blue color indicates the electrophilic, while red one is for nucleophilic nature of the region. The ESP surface of the title molecule indicate that while regions having the negative potential are over the electronegative fluorine atoms (negative regions are usually associated with the lone pair of electronegative atoms) and at the top of nitrogen in amide group, positive ones are over the hydrogen atoms especially near the NH_2 group. The fluorine atoms have electron rich while around the hydrogen atoms correspond to the electron deficient region (especially H atoms of amide group). The maximum values negative and positive potential corresponding to the nucleophilic and electrophilic region, respectively. The surface diagram enable us to visualize the charge distributions, charge related properties of the title molecule, and size and shape of the title molecule.

4.4.4. Mulliken atomic charges

Mulliken atomic charges arise from the Mulliken population analysis [91] and provide a mean of estimating partial atomic charges from calculations carried out by the methods of computational chemistry performed in Gaussian. A reactive atomic charge plays an important role in the application of quantum mechanical calculations of the molecular system. The Mulliken atomic charges of aniline and 2,5-DFA molecule are performed using DFT/B3LYP method with 6-311++G(d,p) and 6-31G(d) basis sets to ensure the best estimation of charges because the Mulliken charge analysis may fail in some cases where the large diffuse functions used in calculations. The Mulliken atomic charges of aniline and 2,5-DFA molecules are gathered in Table S3. Comparison of charges obtained through two basis sets show that; although the sign of the charges for the carbon atoms on the ring altered, that for hydrogens on the ring, the substituent fluorine atoms, and the amino group do not changed. Charge values for substituents are only changed in magnitude. Charge distribution of the molecule is evaluated based on aniline molecule. Results showed that fluorine atoms lead to a redistribution of electron density of aromatic carbon atoms. The distributions of hydrogen in NH_2 groups are similar for aniline molecule. However, the magnitude of the charges of H atoms increases due to high electronegativity of neighboring F atom. Atomic charges for the ring carbons are estimated as negative for aniline whereas there is an alternation in 2,5-DFA molecule due to substitution of F atoms.

4.5. Thermodynamic properties

To see change of thermodynamic properties (heat capacity (C), entropy (S), and enthalpy (H)) with different temperature from 100 to 700 K of the working molecule are obtained from the theoretical harmonic frequencies based on vibrational analysis. The results of statically thermodynamic functions are collected in Table S4, due to the fact that the molecular vibrational intensities increase with temperature. The relations between temperature and heat capacity, entropy, enthalpy changes are plotted in Fig. S6 and fitted by quadratic formulas with their fitting factors (R^2), respectively. The corresponding fitting equations and R^2 values are listed the following, respectively;

$$C = -1.81802 + 0.12408T - 6.6338 \times 10^{-5}T^2 \ (R^2 = 0.9999)$$

$$S = 50.1282 + 0.12460T - 3.3284 \times 10^{-5}T^2 \ (R^2 = 0.9999)$$

$$\Delta H = -0.55388 + 0.00918T + 3.5300 \times 10^{-5}T^2 \ (R^2 = 0.9997)$$

Nonlinearity of thermodynamic parameters results mostly from the temperature dependency of vibrational partition function. The total heat capacity, thermodynamical energy, and the entropy of the molecules are calculated from four basic contributions; electronic, translational, rotational, and vibrational. Quantum chemistry calculations in Gaussian treat the electronic contribution without temperature dependency. All remaining contributions are threated within a certain temperature dependency. Because the partitions functions are directly related to degrees of freedom of the

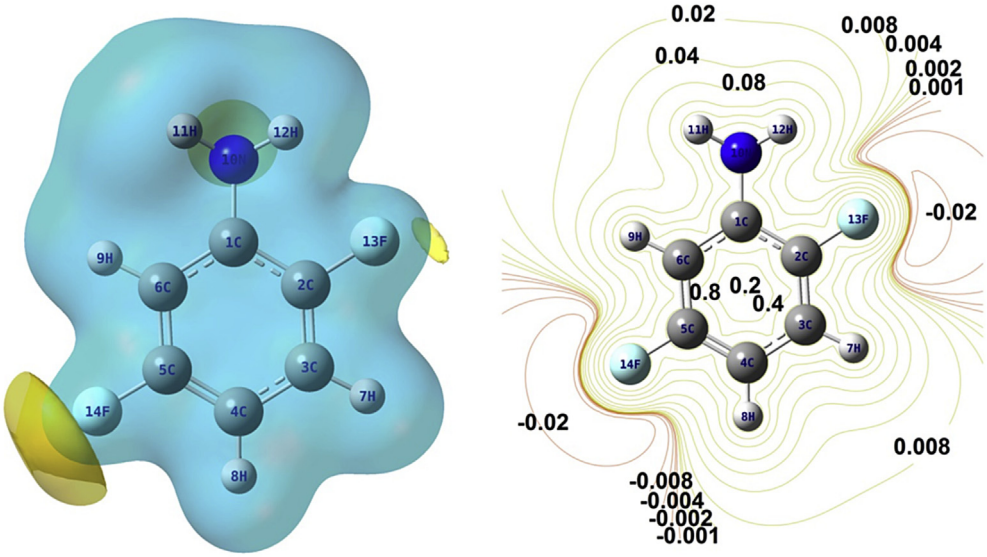

Fig. 6. The electrostatic potential (ESP) graph for 2,5-DFA molecule.

system, the vibrational contributions become dominating factor in polyatomic molecules. Vibrational partition function contains second order exponential terms and the other thermodynamic parameters contain quadratic temperature dependency, thus resulting in nonlinear temperature dependency of thermodynamic parameters due to the nature of calculations. Further studies on 2,5-DFA molecule are presented to supply helpful information for thermodynamical properties. To see and obtain other thermodynamic energies according to relationships of thermodynamic functions and directions of chemical reactions according to the second law of thermodynamics in thermochemical field can be used.

4.6. Reduced density gradient- RDG

To investigate a weak interactions in real space based on the electron density and its derivatives were published an approach by Johnson and co-workers [92]. RDG is dimensionless quantity defined as, obtained density and its first derivative, follows:

$$RDG(r) = \frac{1}{2(3\pi^2)^{1/3}} \frac{|\nabla\rho(\mathrm{r})|}{\rho(\mathrm{r})^{4/3}}$$

The region with low electron density and low RDG value indicate weak interactions. The plots of RDG versus ρ (density values of the low-gradient spike) appear to be an indicator of the interaction strength. The electron density ρ (plot of the RDG versus) multiplied by the sign of λ_2 can permit investigation and visualization of a wide range of interactions types. The sign of λ_2 is used to discriminate bonded ($\lambda_2<0$) from nonbonding ($\lambda_2>0$) interactions. The RDG calculations are performed by Multiwfn [45], and plotted by VMD program [46], respectively.

The electron density value at the RDG versus sign $(\lambda_2)\rho$ peaks itself provides the information about the strength of interaction. There is one spike in the low-density, low gradient region as seen in Fig. S7, indicative of weak interactions in the system for 2,5-DFA molecule, defined different color. The negative values of sign (λ_2) ρ are indicative of stronger attractive interactions. The RDG = 0.2 lines cross not only the attractive but also the repulsion spikes. Large, negative values of sign $(\lambda_2)\rho$ are indicative of stronger attractive interactions, while positive ones strong repulsion interactions. The strength of weak interactions have positive correlations with electron density ρ in corresponding region, Van der Waals interaction regions always have very small ρ, while the regions correspond to strong steric effect and hydrogen bond always have relative large ρ. The regions are identified by color as different type seen from Fig. S8. The color from blue to red means from stronger attraction to repulsion, respectively. The center of rings for 2,5-DFA molecule showed that strong steric effect, filled by red color. The green color circles can be identified as Van der Waals interaction region, means that density electron in these regions are low. The RDG of the molecule are contributed in literature.

4.7. NMR spectra

NMR spectroscopy is one of the principal techniques used to obtain chemical, physical, and structural information about organic molecules. To interpret and predict the even structure of large biomolecules the NMR spectroscopic technique and computer simulation methods offers a powerful way with together [93,94]. ^{1}H and ^{13}C NMR spectra are recorded due to providing more information (utility practical and extensive) about 2,5-DFA molecule. ^{1}H and ^{13}C NMR analysis of the molecule are given both experimentally and theoretically. The experimental results of ^{1}H and ^{13}C NMR spectra of the present molecule are given in Fig. 7a and b, respectively. The experimental and calculated NMR data (^{1}H and ^{13}C NMR) in $CDCl_3$ solvent are tabulated in Table 3. The atom positions are listed according to number of Fig. 1.

Gauge-including atomic orbital [47,48] method are employed for ^{1}H and ^{13}C NMR chemical shifts calculations of the present molecule after the full geometry optimization by the DFT/B3LYP/6-311G++(d,p) basis set. The GIAO approach to molecular systems was essentially developed by an efficient application method of ab-initio SCF calculations, by using techniques taken from analytic derivative methodologies [47,48]. The location of chemical shifts (peaks) on an NMR spectrum is measured from a reference point that the hydrogen in a standard reference compound TMS—produce.

There are two type hydrogen atoms of the studied molecule (in NH_2 and phenyl ring). Phenyl ring protons of organic molecules usually have seen in the range of 7.00–8.00 ppm. The chemical shifts of proton vary in their electronic environment. The hydrogen, attached or nearby electron-withdrawing atom or group, can decrease the shielding and move the resonance of attached proton towards to a higher frequency, while a lower frequency, attached electron-donating atom or group [95]. The proton chemical shifts are recorded in the range of 6.31–6.91 ppm (ring) and at 3.80 ppm (NH_2) for 2,5-DFA molecule. The protons attached electron-withdrawing atom (N) decreased the shielding and resonance for the title molecule. The chemical shifts of NH protons in generally would be more susceptible to intermolecular interactions as compared other heavier atoms [96]. Therefore, the NH proton signal varies greatly with concentration and solvent effects and occasionally cannot be seen in the spectra or resonance. For 2,5-DFA molecule; the chemical shifts value of H8 smaller than the other phenyl ring protons, due to the near the electron-donating atom F14 atom. The calculated theoretical values are dropped nearly the same region for phenyl ring, showed well agree.

The aromatic carbons chemical shift values give resonances and overlap areas from 100 to 150 ppm in NMR spectra [97–99]. The chemical shift values of carbon atoms (in phenyl ring) in the title molecule were the same parallel with this range and well agreement. However the chemical shift values of the carbon atoms C2, C5 (2,5-DFA), bonded F atoms are bigger than other carbons. The C4 and C6 atoms have smaller chemical shifts (both experimental and theoretical) than the other ring carbon atoms, due to electronic environment of C4 (near the F atoms) and C6 atom (near the NH_2 group and F atoms). The literature are also supported in our experimental and theoretical results for the this structurally similar molecules [32,33,100]. Some differences between experimental and theoretical values (~8 ppm for C5, ~5 ppm for C2 and C3) were recorded. True estimation of shielding in the regions near fluorine atoms is not as good as the estimation for the other regions. Because fluorine atoms are highly sensitive to magnetic field, some uncounted effects exist in fluorine substituted molecules.

The ^{1}H and ^{13}C NMR correlation graphics were presented one by one in Fig. 8a and b, respectively. The following equations express that the relations between the experimental and theoretical chemical shifts of the molecule:

For ^{1}H: δ_{exp} (ppm) = $0.9079\delta_{cal}$–0.4988 ($R^2 = 0.9953$)

For ^{13}C: δ_{exp} (ppm) = $0.8939\delta_{cal}$ + 8 .9690 ($R^2 = 0.9995$)

^{1}H and ^{13}C NMR results gave a good coefficient and lower standard error as $R^2 = 0.9953$ and $R^2 = 0.9995$, respectively. The ^{1}H and ^{13}C chemical shifts data, given in Table 3, can be seen well agree. However, very small differences are considered between experimental and theoretical these can occurred solvent effects, and local magnetic field effect.

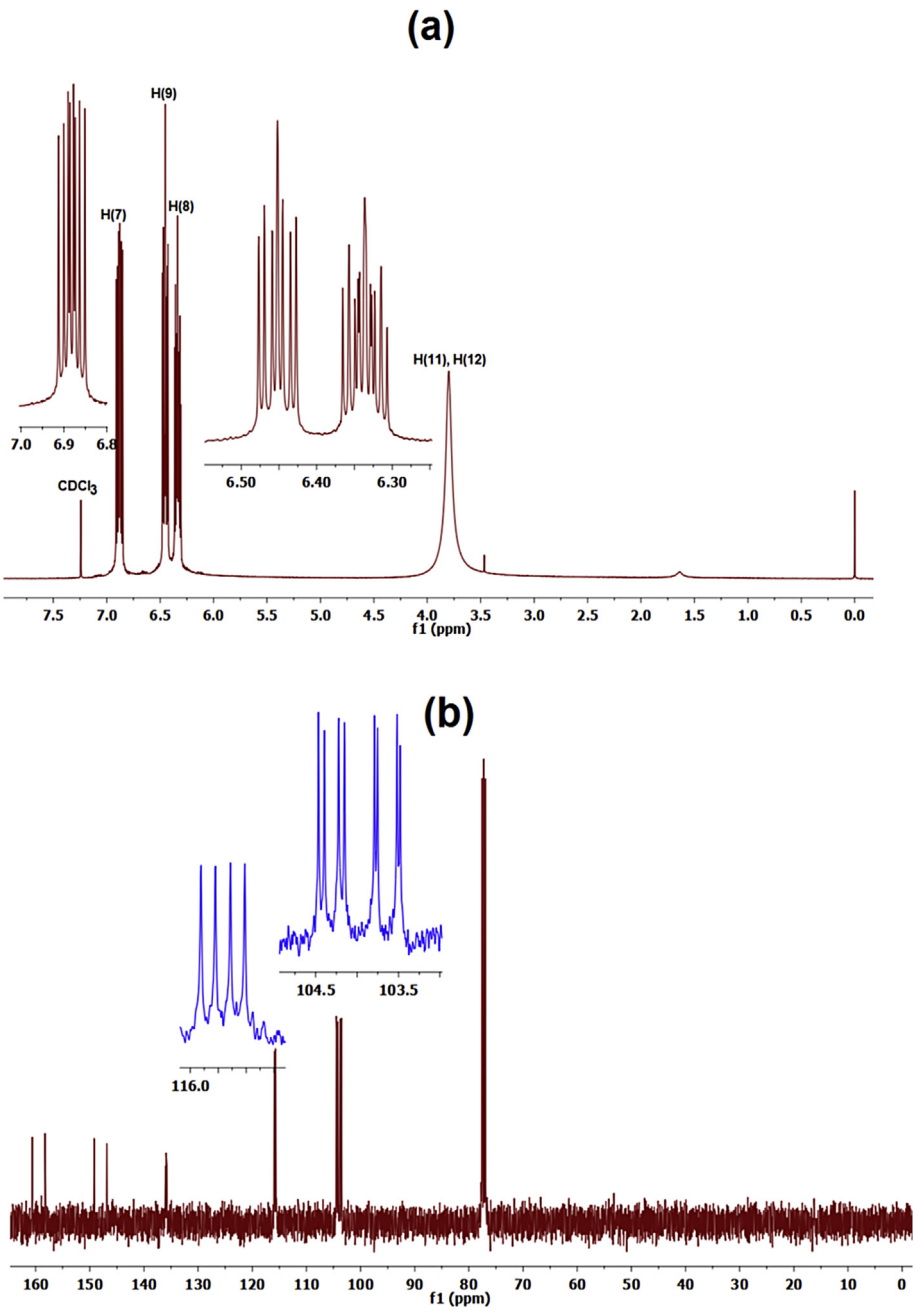

Fig. 7. (**a**) ^{1}H NMR (**b**) ^{13}C NMR spectra of 2,5-DFA.23DFA in $CDCl_3$ solution.

Table 3
Experimental and theoretical, ^{1}H and ^{13}C NMR isotropic chemical shifts (with respect to TMS) of 2,5D-FA with DFT (B3LYP 6-311++G (d,p)) method.

Atom	Exp.	Theoretical	Atom	Exp.	Theoretical
C (1)	135.69–136.03	142.81	H (7)	6.85–6.91	7.04
C (2)	146.84–149.16	155.03	H (8)	6.31–6.37	6.35
C (3)	115.61–115.92	120.02	H (9)	6.43–6.48	6.61
C (4)	104.15–104.47	106.05	H (11)	3.80	3.50
C (5)	158.25–160.63	168.07	H (12)	3.80	3.79
C (6)	103.48–103.79	105.81			

4.8. Vibrational spectral analysis

This section gives to make a comparison with the results of the theoretical calculations and the experimental results and structurally similar molecules. The spectroscopic signature of 2,5-DFA molecule and the assignments of the vibrational spectra of the title molecule provide helpful and realistic accommodation. Theoretical results are obtained from DFT/B3LYP method, 6-311G++(d,p) basis set. The theoretical results are higher than the experimental ones. The discrepancy may be a consequence of the anharmonicity and general tendency of the quantum chemical methods to overestimate the force constants at the exact equilibrium geometry. The theoretical calculations have obtained in vacuum, while experimental ones for liquid state is other probability. To eliminate this differences, the theoretical vibrational frequencies are multiplied by the scale scaling factor [40]. The vibrational (FT-IR and FT-Raman) spectra of the title molecule (with the scaling factor) are given in Figs. 9 and 10.

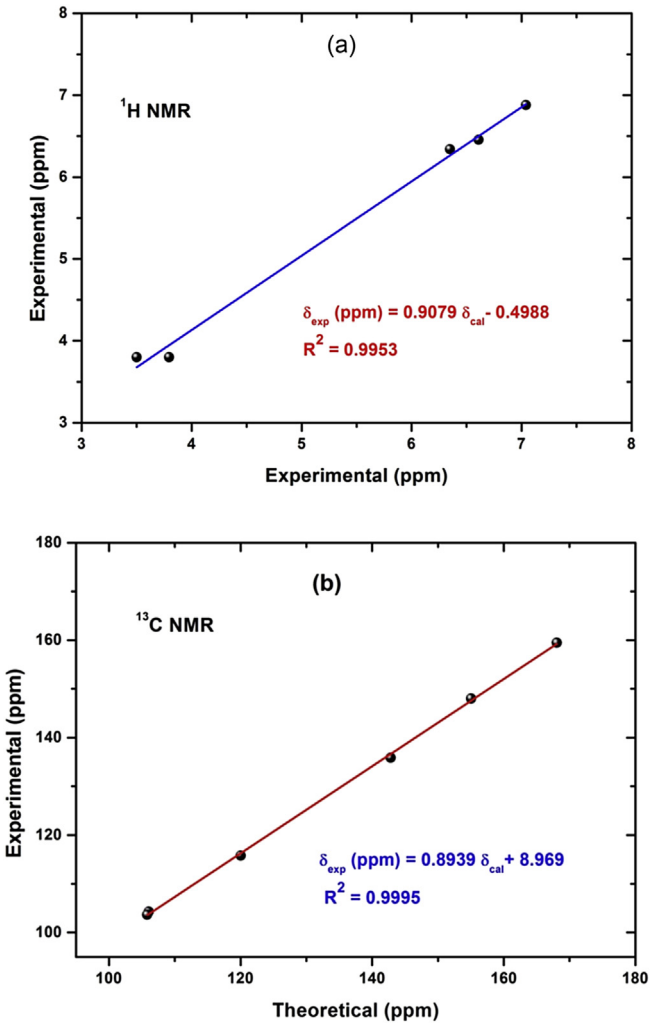

Fig. 8. Correlation graphic of **a)** proton NMR and **b)** carbon NMR of 2,5-DFA.

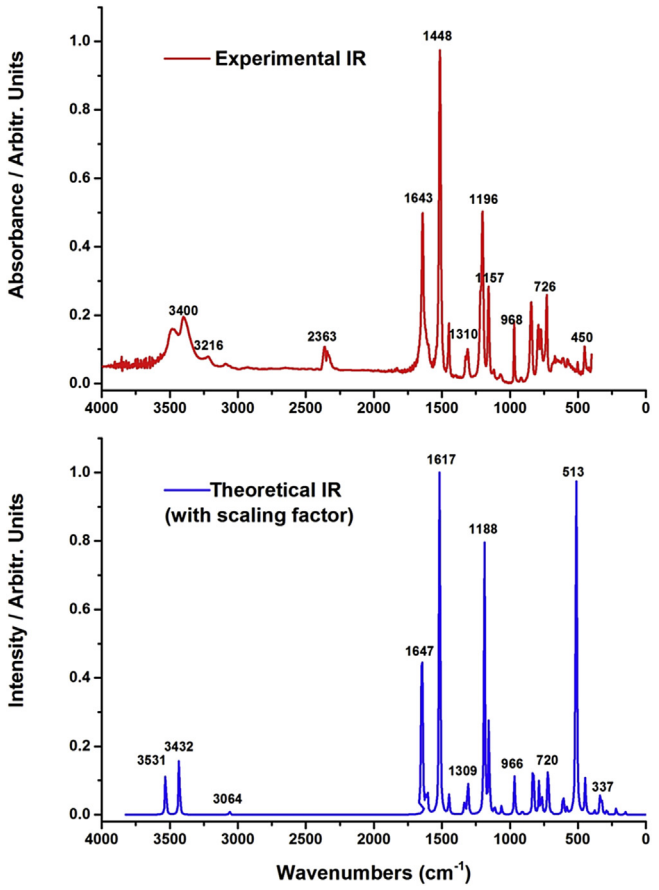

Fig. 9. The calculated (with the scale factor) and experimental FT-IR spectra of 2,5-DFA.

2,5-DFA molecule has C_1 point group symmetry; consist of 14 atoms, so they have (3N-6) 36 fundamental vibrational modes. These vibrational modes are spanning irreducible representations: 36 and are non-planar structures in the C_1 point group symmetry (A species). There is imaginary frequency (370.57i cm^{-1}), based on C_s point group symmetry of the molecule. Therefore, we used C_1 point group symmetry of molecule for all calculations. The vibrational (FT-IR and FT-Raman) wavenumbers both experimental and theoretical and its assignments with PED of 2,5-DFA molecule are presented in Table 4.

4.8.1. NH_2 (amino group) vibration modes

The molecule 2,5-DFA consisting of a phenyl group attached to an amino group (NH_2), aniline and its derivatives are the prototypical aromatic amine. The amino groups generate two (N–H) stretching modes, as asymmetric and symmetric. Asymmetric modes generally are seen higher region than symmetric ones. The N–H stretching modes also were obtained at 3418-3515 cm^{-1} (vapor), 3401, 3485 cm^{-1} (solution) and 3360, 3440 cm^{-1} (liquid) for infrared spectrum and 3360, 3435 cm^{-1} (liquid) for Raman spectrum of aniline [9]. The N–H stretching vibrations usually occur in the region 3300–3500 cm^{-1} in primary amines [30–34]. The N–H stretching frequencies were observed at 3432, 3366 cm^{-1} in ortho-, 3440, 3376 cm^{-1} in meta- and 3425, 3370 cm^{-1} in para-fluoroanilines [24]. Honda et al. assigned the asymmetric and symmetric NH_2 stretching vibrations modes at 3508 and 3421 cm^{-1} in IR spectrum of aniline, at lower frequencies 3499 and 3414 cm^{-1} for para-fluoroaniline, respectively [28]. These modes were recorded at 3450/3446 cm^{-1} and 3351/3339 cm^{-1} in FT-IR/FT-Raman spectra of 3,5-DFA, assigned to asymmetric and symmetric NH_2 stretch modes, respectively [33]. Theoretical wavenumbers corresponding to these modes are at 3528 cm^{-1} and 3431 cm^{-1}, respectively [33]. The N–H stretching modes of *m*-methylaniline were observed at 3435/- and 3354/3353 cm^{-1} in FT-IR/FT-Raman spectra, assigned to asymmetric and symmetric, respectively [101]. In this study, the modes number ν1 and ν2 assigned asymmetric and symmetric modes, respectively. These modes are calculated at (symmetric/asymmetric) 3432/3531 cm^{-1}, respectively for 2,5-DFA molecule. The experimental results are seen at 3400/3433 cm^{-1} in FT-IR spectrum and in FT-Raman spectrum, only one peak is observed at 3366 cm^{-1} N–H symmetric modes for 2,5-DFA molecule.

The amino group have a broad NH_2 scissoring, rocking, wagging (inversion) and torsional vibrational modes, in addition to the N–H stretching modes. The N–H scissoring modes were observed in the region 1610–1630 cm^{-1} [102]. Two N–H scissoring bands (according to the PED) were obtained at 1620 and 1630 cm^{-1}, in IR spectrum of 4FA [24]. The modes were at 1645 and 1630 cm^{-1} assigned NH_2 scissoring motion and observed at 1655 and 1639 cm^{-1} in FT-IR spectrum, at 1662 and 1633 cm^{-1} in FT-Raman spectrum of 3,5-DFA molecule by Pathak et al. [33]. In this paper, we predicted two N–H scissoring modes (ρNH_2) at 1617 and 1647 cm^{-1}

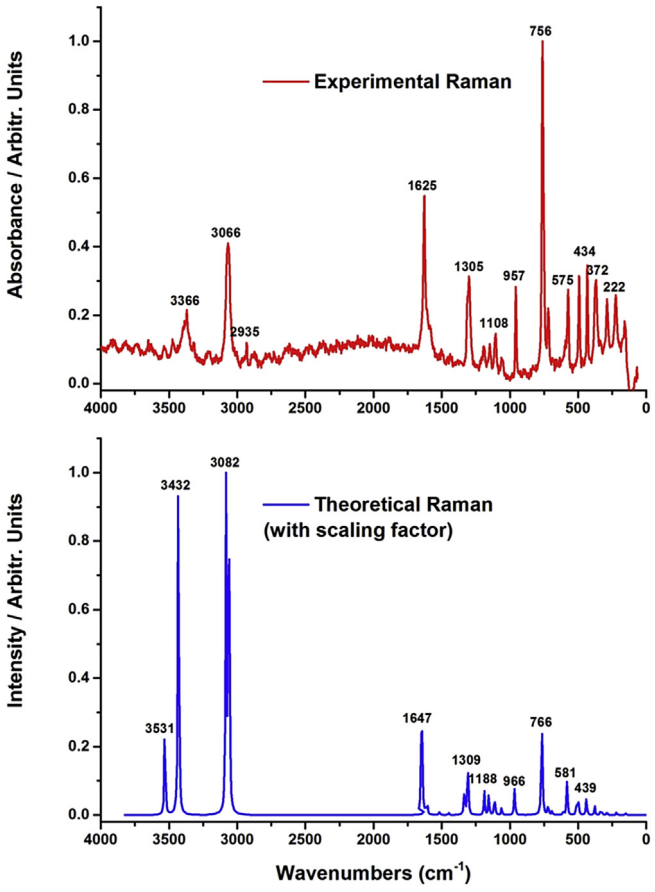

Fig. 10. The calculated (with the scale factor) and experimental FT-Raman spectra of 2,5-DFA.

(2,5-DFA), recorded at 1625 and 1643 cm^{-1} in FT-Raman and FT-IR, respectively.

The modes, assigned NH_2 rocking, are mixed modes the other in plane and stretching modes. The mode number ν17 (2,5-DFA) which is contributed largest one according to their PED (37%). The rocking mode of the amino group in the title molecule is calculated in the region nearly 1000–1300 cm^{-1} which are in good agreement with the assigned NH_2 rocking in the literature [18,32–34,56–58].

The NH_2 wagging vibration modes is predicted at 513 cm^{-1} for 2,5-DFA molecule in this paper. These modes were assigned inversion NH_2 and computed at 517 cm^{-1} for 2,3-DFA, 559, 574 cm^{-1} for 2,4-DFA molecule [34]. 2,4-DFA molecule have bigger values than 2,3-DFA [34] and 2,5-DFA molecule (in this study). This result can be the position of fluorine atom at para position of 2,4-DFA molecule. The NH_2 inversion (wagging) mode was found to be 493 cm^{-1} with PED of 74% was well matched with experimental value at 485 cm^{-1} [33]. The amino group wagging vibration was predicted as the strongest IR intensity band at each type of calculations considered. However, this mode appeared as a very broad structure less band with medium intensity in the 740–520 cm^{-1} region of experimental IR spectrum and too weak to determine in Raman spectrum [103]. López-Tocón et al. [27] assigned NH_2 inversion, (γNH_2 wagging) at 621 cm^{-1} for 4FA molecule. The bands at 553 cm^{-1} (FT-IR) and 342 cm^{-1} (FT-Raman) were predicted as wagging mode of NH_2 [32]. Similar structural molecules [29,30,59,60,104], are showed nearly the same results and agree well for these modes.

4.8.2. Phenyl ring and substituent vibration modes

To identify C–NH_2 stretching modes from other vibrations modes is rather difficult task [105]. The C–NH_2 stretching modes were assigned in the region 1386–1266 cm^{-1} for aromatic amines by Silverstein [102]. In the infrared spectrum of liquid aniline the band of medium intensity at 1278 cm^{-1} was assigned to the C–NH_2 stretching mode [9]. The band at ca. 1279 cm^{-1} in the experimental spectrum corresponded to the C–N stretching mode [18]. The region 1200–1300 cm^{-1} was assigned as C–NH_2 stretching vibrations for ortho-, meta- and para-fluoroanilines [24]. The C–N stretching mode ν(C–NH_2) was assigned at 1274 cm^{-1} in Raman spectrum of 4FA [27]. The medium intensity band at 1273 cm^{-1} in IR spectrum of 4FA (1275 cm^{-1} in Raman) was assigned to C–N vibrations [60]. The C–N mode was assigned as the C–N stretching, observed (FT-IR and Raman) at 1293 cm^{-1} for *m*-methylaniline [106] observed at 1267 cm^{-1} (IR) [1271 cm^{-1} (Raman)] for *p*-methylaniline [107]. In this study, the C–NH_2 stretching modes dispersed in the board region and contaminated the other modes. The dominant mode of these vibrations corresponding calculated scaled wavenumbers at 1309 cm^{-1} in good correlation with experimental values (1310 cm^{-1} in FT-IR and 1305 cm^{-1} in FT-Raman) for 2,5-DFA molecule. τCCCN torsion modes are coupled with C–H or C–F out of plane vibration modes (see Table 4). The δCCN modes are calculated at 288 cm^{-1} (at 286 cm^{-1} in FT-Raman) corresponding dominant modes for 2,5-DFA molecule. The assignments are supported by their PEDs.

There are two fluorine atoms in present molecule. The C–F stretching modes are no pure, combined with other vibrations especially ring modes. The C–F stretching modes are seen broad band in Table 4. The biggest percentages of this mode is ν_{14} as 45% for 2,5-DFA molecule. The largest mode is calculated at 1188 cm^{-1} in good correlation with their FT-IR and FT-Raman spectra of the molecule. Two C–F stretching modes, strongly coupled with C–N, C–C stretching and C–H in plane bending were assigned at 1355/1348 cm^{-1} and 1115/1113 cm^{-1} in FT-IR/FT-Raman spectra of 3,5-DFA. These modes were calculated at 1350 cm^{-1} and 1105 cm^{-1} by using B3LYP/6-311++G(d,p) basis set Karabacak et al. [33]. The C–F stretching vibration bands were seen at 1210 and 998 cm^{-1} for 2,5-DFA [108]. The dominant contribution modes were assigned C–F stretching at 1206 cm^{-1} (2FA), 1146 cm^{-1} (3FA) and 1223 cm^{-1} (4FA) and computed at 1194, 1152 and 1223 cm^{-1} for 2FA 3FA and 4FA, respectively as the strong and broad IR bands [60]. These modes were obtained in the region 1232–1109 cm^{-1} for 2,4,5-TFA, 1353 and 1113 cm^{-1} for 2,4,6-TFA molecule [59]. The frequencies in the range of 1000–1350 cm^{-1} were recorded to have comparatively less intensities in the IR spectrum, but, with the help of PEDs were assigned at 1236, 1020 and 980 cm^{-1} for 2,3,4-TFA and 1260, 1041 and 924 cm^{-1} for 2,3,6-TFA to three C–F stretching vibrations [30].

The C–F in-plane bending modes were appeared at 535 cm^{-1} and 321 cm^{-1} matched well with FT-IR spectral value at 539 cm^{-1} [33]. One of three C–F in-plane bending modes was found at ~620 cm^{-1} [28] and ~595 cm^{-1} [30] for derivatives of substituted fluoroaniline molecules. The in-plane C–F bending vibrations were found in the range of 266–318 cm^{-1} [109]. Similarly, a frequencies ~435 cm^{-1} had been assigned to the C–F in-plane bending vibration for several mono-fluoroanilines [24,108]. Weak band at 567 cm^{-1} and 505 cm^{-1} in FT-IR spectrum of 2,3-DFA and 2,4-DFA, respectively are assigned as C–F in plane bending, well matched with theoretical values 560 cm^{-1} and 498 cm^{-1}. Other C–F in-plane bending mode is calculated at 284 cm^{-1} for 2,3-DFA and 324 cm^{-1} for 2,4-DFA respectively [34]. In the present case, the C–F in-plane bending vibration modes of the headline molecule were calculated especially two regions near 300-350 and 500–590 cm^{-1}. The largest contribution were seen at 337 cm^{-1} (60%) for 2,5-DFA molecule.

Table 4
Comparison of the calculated harmonic frequencies and experimental (FT-IR and FT-Raman) wavenumbers (cm^{-1}) using by B3LYP method 6-311++G(d,p) basis set of 2,5-DFA molecule.

Modes	Theoretical		Experimental		PED[a] (≥10%)
No	Unscaled freq.	Scaled freq.	FT-IR	FT-Raman	
ν1	3685	3531	3433(w)		$\nu NH_{2\ asym.}$ (100)
ν2	3582	3432	3400(w)	3366(w)	$\nu NH_{2\ sym.}$ (100)
			3216 (vw)		overtone + combination
ν3	3217	3082	3090 (vw)		$\nu CH_{sym.}$ (99)
ν4	3198	3064		3066(m)	$\nu CH_{asym.}$ (100)
ν5	3191	3057		2935 (vw)	$\nu CH_{asym.}$ (100)
			2363(w)		overtone + combination
			2342(w)		overtone + combination
ν6	1676	1647	1643(s)		νCC (54), ρNH_2 (20), δCCC (10)
ν7	1645	1617		1625(s)	ρNH_2 (59), νCC (24)
ν8	1634	1606	1600(w)		νCC (56), δCCC (21)
ν9	1542	1516	1514 (vs)		δCCH (40), νCC (31), δCCC (10)
ν10	1474	1449	1448(w)		δCCC (36), δCCH (22), νCN (17)
ν11	1357	1334	1328 (vw)		νCC (86)
ν12	1331	1309	1310(w)	1305(m)	νCC (34), νCN (24), νCF (18), δCCH (13)
ν13	1284	1262			δCCH (68), νCC (10), rNH_2 (10)
ν14	1208	1188	1196(s)	1192(w)	νCF (45), δCCC (22), νCC (11), rNH_2 (10), δCCH (10)
ν15	1175	1155	1157(m)	1148(w)	δCCH (34), νCF (31), νCC (17), νCN (10)
ν16	1132	1112	1118 (vw)	1108(w)	δCCH (55), νCC(20), rNH_2 (16)
ν17	1078	1060	1065 (vw)	1060(w)	rNH_2 (37), δCCH (22), δCCC (19)
ν18	982	966	968(m)	957(m)	νCC (37), δCCC (27), δCCH (13), νCF (11)
ν19	924	908	914 (vw)		γCH (97)
ν20	844	830	842(m)		γCH (83), τCCCF (10)
ν21	800	787	790(m)		γCH (81), τCCCF (13)
ν22	779	766	769(m)	756 (vs)	νCC (45), νCF (18), δCCC (23)
ν23	732	720	726(m)	720(w)	δCCC (47), νCF (34)
ν24	703	691	670 (vw)		γCH (41), τCCCN (37), τCCCF (19)
ν25	620	609	611 (vw)		γCH (46), τCCCF (37), τCCCN (14)
ν26	591	581	578 (vw)	575(m)	δCCC (33), δCCF (33), νCC (19)
ν27	522	513			ωNH_2 (76)
ν28	508	499	500 (vw)	494(m)	δCCC (41), δCCN (25), δCCF (15), νCC (10), νCN (10)
ν29	455	447	450(w)		γCH (68), τCCCF (15), τCCCN (14)
ν30	446	439		434(m)	δCCC (70), δCCF (20)
ν31	385	378		372(m)	τCCCF (57), ϕNH_2 (32)
ν32	342	337			δCCF (60), ϕNH_2 (16)
ν33	331	325			ϕNH_2 (63), δCCF (19), τCCCF (10)
ν34	292	288		286(w)	δCCN (49), δCCF (23), δCCC (11), νCC (11)
ν35	222	218		222(w)	τCCCC (62), τCCCN (19), τCCCF (17),
ν36	154	152		154 (vw)	τCCCC (85), τCCCF (12)

[a] PED: Potential Energy Distribution. ν; stretching, γ; out-of plane bending, δ; in-plane-bending, τ; torsion, ρ; scissoring, ω; wagging, ϕ; twisting, r; rocking.

The modes of the C–F out-of-plane bending vibrations are predicted at 152, 218, and 378 cm^{-1} for 2,5-DFA by using DFT/B3LYP/6-311G++(d,p) basis set. These mode are not observed FT-IR spectrum due to the not include in these region. FT-Raman spectrum of the title molecule are in very good coherent (as 154, 222 and 372 cm^{-1}) with the theoretical results. The results are also good consistency with in the literature [28,30,34,59,110]. The other torsion modes of the related fluorine atom are seen in Table 4.

The familiar and common vibration mode of aromatic phenyl ring is C–C stretching. They are very considerable and also very characteristic for the aromatic phenyl ring. Varsanyi [111] observed at 1625–1590, 1590–1575, 1540–1470, 1465–1430 and 1380–1280 cm^{-1} from the frequency ranges for the five bands and impressed that the bands were of variable intensity. The C–C stretching vibrations modes are assigned in the region 1647–1516, 1334–1112, 966, 766, 581, and 499 cm^{-1} for 2,5-DFA molecule. The biggest contribution comes from modes number ν_{11} (86%). The values of C–C stretching modes are good agreement with their experimental (FT-IR and FT-Raman) vibrational results.

The assignment shown in Table 4 for several of bending and torsion modes such as: CCC bending (as seen ring deformation) was meddled with other modes and sometimes missing in FT-Raman spectrum. The purest contribution of CCC bending modes (ν30) are obtained at 439 cm^{-1} with scaling factor for the 2,5-DFA molecule. This mode is in good agreement with experimental value is recorded at 434 cm^{-1} in Raman spectrum.

The C–H stretching modes of phenyl ring seemed as poly peaks in the 3000–3100 cm^{-1} range, which is the typical region [112]. The C–H stretching vibration modes of phenyl ring are calculated in the range of 3057–3082 cm^{-1} by using the DFT/B3LYP/6-311++G(d,p) method and observed at 3090 cm^{-1} (in FT-IR), 2935 and 3066 cm^{-1} (in FT-Raman), respectively. The contribution of the modes are very pure nearly 100% according to their PED. These regions for aniline molecule, which is base structure of the title molecule, were presented as 3025–3094 cm^{-1} (vapor), 3013–3094 cm^{-1} (solution), 3010–3088 cm^{-1} (liquid) in infrared spectrum and 3010–3072 cm^{-1} (liquid) in Raman spectrum, respectively [9]. The C–H stretching modes were recorded in the region 3035–3106 cm^{-1} in FT-IR and 3054–3109 cm^{-1} in FT-Raman spectra [113]. The frequencies were also recorded for many fluorine derivatives of aniline molecules in the same region [25,29–31,33,34,60].

The in plane and out-of-plane bending C–H vibrations record in the range of 1000–1300 cm^{-1} and 750–1000 cm^{-1}, respectively [112]. The C–H in plane bending modes for aniline molecule were recorded in the region 1028–1180 cm^{-1} (vapor), 1028–1308 cm^{-1} (solution), 1028–1312 cm^{-1} (liquid) in the infrared spectrum and 1029–1176 cm^{-1} (liquid) in Raman spectrum respectively. Out-of-

plane bending C–H vibration modes were observed in the region 740–874 cm^{-1} (vapor), 747–968 cm^{-1} (solution), 751–970 cm^{-1} (liquid) in infrared spectrum and 755–970 cm^{-1} (liquid) in Raman spectrum, respectively [9]. In this work, the C–H in plane bending vibrations modes are predicted and observed (FT-IR/FT-Raman) nearly at 950–1520 cm^{-1}. However, the C–H in-plane modes are generally coupled or contaminated the CC stretching modes. The C–H out-of-plane bending vibrations modes are calculated at 447, 609, 691, 787, 830, and 908 cm^{-1} for the present molecule in well agreement their experimental (FT-IR) results. The results shows very good coherent with experimental data (FT-IR).

The torsion modes are assigned in the broad band and contaminated other modes and also named as out-of plane modes of C–H, O–H, and C–F, required no further discussion, therefore, an analysis is given these section.

hyperpolarizability and dipole moment of the title molecule are proved in this study. Polarizability and hyperpolarizability tensors (α_{xx}, α_{xy}, α_{yy}, α_{xz}, α_{yz}, α_{zz} and β_{xxx}, β_{xxy}, β_{xyy}, β_{yyy}, β_{xxz}, β_{xyz}, β_{yyz}, β_{xzz}, β_{yzz}, β_{zzz}) of the molecule are obtained by Gaussian output job file of frequency. The units of them (α and β) are converted into from (Gaussian output) in atomic units (a.u.) to electronic units (esu) [for α; 1 a.u. = 0.1482×10^{-24} esu, for β; 1 a.u. = 8.6393×10^{-33} esu]. The following equations are calculated the mean polarizability (α), anisotropy of polarizability ($\Delta\alpha$) and the average value of the first hyperpolarizability $\langle\beta\rangle$.

$$\alpha_{tot} = \frac{1}{3}\left(\alpha_{xx} + \alpha_{yy} + \alpha_{zz}\right)$$

$$\Delta\alpha = \frac{1}{\sqrt{2}}\left[\left(\alpha_{xx} - \alpha_{yy}\right)^2 + \left(\alpha_{yy} - \alpha_{zz}\right)^2 + \left(\alpha_{zz} - \alpha_{xx}\right)^2 + 6\alpha_{xz}^2 + 6\alpha_{xy}^2 + 6\alpha_{yz}^2\right]^{\frac{1}{2}}$$

$$\langle\beta\rangle = \left[\left(\beta_{xxx} + \beta_{xyy} + \beta_{xzz}\right)^2 + \left(\beta_{yyy} + \beta_{yzz} + \beta_{yxx}\right)^2 + \left(\beta_{zzz} + \beta_{zxx} + \beta_{zyy}\right)^2\right]^{\frac{1}{2}}$$

The best way to evaluate the correlation between the experimental and calculated frequencies is to plot. Therefore, Fig. 11 is given to show and evaluate to infrared spectrum of the title molecule. The relationship is described as linear given following equation:

$$\nu_{exp.}\,(cm^{-1}) = 0.9818\nu_{cal.} + 14.464\ (R^2 = 0.9994)$$

4.9. Nonlinear optical properties and dipole moment

The molecular polarizability, anisotropy of polarizability, first

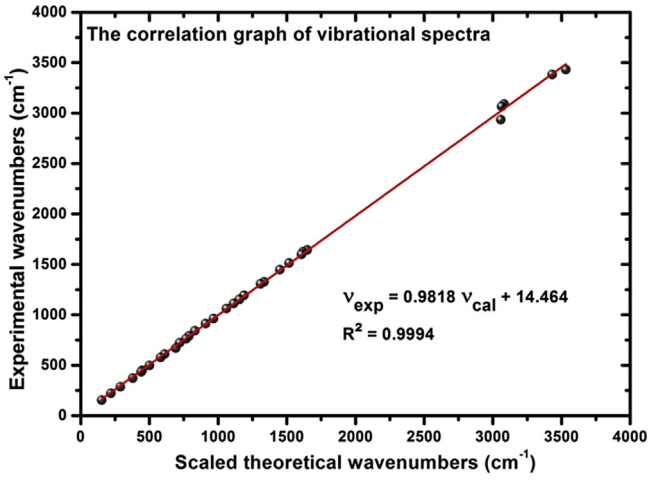

Fig. 11. The correlation graphic of calculated and experimental frequencies of 2,5-DFA.

The electronic dipole moment μ_i (i = x, y, z) and total dipole moment μ_{tot}, are calculated given the next equation, of the studied molecule are gathered in Table S5.

$$\mu_{tot} = \left(\mu_x^2 + \mu_y^2 + \mu_z^2\right)^{\frac{1}{2}}$$

The higher values of dipole moment, molecular polarizability, and hyperpolarizability are important and well known for more active NLO properties. The relatively homogeneous charge distribution of molecules caused small dipole moment. The total dipole moment is calculated as 1.7927 (2,5-DFA) Debye (D). The components μ_x are highest value of dipole moment for the head molecule μ_z is the smallest one. The polarizability of the title molecule is 11.541553 $\times$ 10^{-24} esu, (2,5-DFA). The anisotropy of the polarizability of the title molecule is listed after polarizability deep of in Table S5. The molecular first hyperpolarizability β is one of important key factors in a NLO system. The first hyperpolarizability value of 2,5-DFA molecule is calculated 2580.7892 $\times$ 10^{-33} esu. The first hyperpolarizability (β) value is 5.2 times bigger than urea values, polarizability (α) value is 2.3 times larger than urea molecule, anisotropy of the polarizability ($\Delta\alpha$) value is 2.7 times larger than urea data, and dipole moment (μ_{tot}) value is 2.2 times larger than those of urea. Therefore, we can say our title molecule shows more polarizability than urea.

5. Conclusions

The experimental and theoretical (DFT) studies are investigated, related on the structural UV–vis, NMR and vibrational (FT-IR and FT-Raman) spectra of 2,5-DFA molecule in this work. The optimized parameters (bond lengths and bond angles) are determined by using B3LYP/6-311++G(d,p) level of theory. These results are compared of the X-ray results of architecture of aniline and similar structures. The mass spectrum of the title molecule is investigated

and showed possible fragments and predicted stable structure. The UV–Vis spectrum is studied for gas phase and different solvents ethanol and water. The frontier molecular, HOMO and LUMO orbitals, density of states, MEPs and Mulliken atomic charges of the molecule are presented. The thermodynamic properties, changing different temperature are given in tables and graphs. The thermodynamic results are increasing with temperature. The RDG studies of the present molecule are achieved. The ^{1}H and ^{13}C NMR spectra of the molecule are recorded by tentative techniques and theoretical method. ^{1}H and ^{13}C NMR theoretical results are showed well agree with their tentative data. They are good correlation each other. The vibrational properties of the studied molecule are obtained by experimental and theoretical quantum chemical methods with their PED. The assignments are also compared with the structurally similar molecules for the most important regions. The NH_2 groups or F atoms have been affected the molecular structure and vibrational frequencies of the title molecule as seen related part of study, leading to further change in the charge distribution in the molecule. Nonlinear optical properties of the title molecule are also obtained from DFT results and evaluated based on results of urea. Eventually if the whole results are looked at form head to foot, they are very well coherent and in agreement.

Acknowledgement

This work is supported by the Celal Bayar University Research fund through research Grant No: FBE–2011/70.

Appendix A. Supplementary data

Supplementary data related to this article can be found at http://dx.doi.org/10.1016/j.molstruc.2016.05.088.

References

[1] S. Gheewala, A. Annachhatre, Water Sci. Technol. 36 (1997) 53–63.
[2] S.E. Manahan, Environmental Chemistry, Taylor & Francis, 2000.
[3] H. Cerecetto, W. Porcal, Mini Rev. Med. Chem. 5 (2005) 57–71.
[4] I. Sánchez, M.D. Pujol, Tetrahedron 55 (1999) 5593–5598.
[5] A. Heaton, M. Hill, F. Drakesmith, J. Fluor. Chem. 81 (1997) 133–138.
[6] A.L. Sharma, S. Annapoorni, B.D. Malhotra, Curr. Appl. Phys. 3 (2003) 239–245.
[7] J. Niessen, U. Schröder, M. Rosenbaum, F. Scholz, Electrochem. Commun. 6 (2004) 571–575.
[8] C.S. Venkateswaran, N.S. Pandya, Proc. Indian Acad. Sci. - Sect. A 15 (1942) 390–395.
[9] J.C. Evans, Spectrochim. Acta 16 (1960) 428–442.
[10] R.A. Kydd, P.J. Krueger, Chem. Phys. Lett. 49 (1977) 539–543.
[11] E. Akalin, S. Akyüz, J. Mol. Struct. 482–483 (1999) 175–181.
[12] M.E. Vaschetto, B.A. Retamal, A.P. Monkman, J. Mol. Struct. Theochem 468 (1999) 209–221.
[13] D.G. Lister, J.K. Tyler, J.H. Høg, N.W. Larsen, J. Mol. Struct. 23 (1974) 253–264.
[14] G. Roussy, A. Nonat, J. Mol. Spectrosc. 118 (1986) 180–188.
[15] G. Schultz, G. Portalone, F. Ramondo, A. Domenicano, I. Hargittai, Struct. Chem. 7 (1996) 59–71.
[16] M. Fukuyo, K. Hirotsu, T. Higuchi, Acta Crystallogr. Sect. B 38 (1982) 640–643.
[17] A.D. Gorse, M. Pesquer, J. Mol. Struct. Theochem 281 (1993) 21–32.
[18] M. Castellá-Ventura, E. Kassab, Spectrochim. Acta A 50 (1994) 69–86.
[19] M. Karabacak, M. Kurt, A. Atac, J. Phys. Org. Chem. 22 (2009) 321–330.
[20] Y. Wang, S. Saebø, C.U. Pittman, J. Mol. Struct. Theochem 281 (1993) 91–98.
[21] A.U. Rani, N. Sundaraganesan, M. Kurt, M. Cinar, M. Karabacak, Spectrochim. Acta A 75 (2010) 1523–1529.
[22] M.A. Palafox, J. Núñez, M. Gil, J. Mol. Struct. Theochem 593 (2002) 101–131.
[23] R.A. Kydd, P.J. Krueger, J. Chem. Phys. 69 (1978) 827–832.
[24] M.A. Shashidhar, K.S. Rao, E.S. Jayadevappa, Spectrochim. Acta A 26 (1970) 2373–2377.
[25] B.B. Lal, G.D. Batuah, I.S. Singh, Curr. Sci. 40 (1971) 655–656.
[26] N.W. Larsen, E.L. Hansen, F.M. Nicolaisen, Chem. Phys. Lett. 43 (1976) 584–586.
[27] I. López-Tocón, M. Becucci, G. Pietraperzia, E. Castellucci, J. Otero, J. Mol. Struct. 565–566 (2001) 421–425.
[28] M. Honda, A. Fujii, E. Fujimaki, T. Ebata, N. Mikami, J. Phys. Chem. A 107 (2003) 3678–3686.
[29] P.M. Wojciechowski, D. Michalska, Spectrochim. Acta A 68 (2007) 948–955.
[30] V. Mukherjee, K. Singh, N.P. Singh, R.A. Yadav, Spectrochim. Acta A 73 (2009) 44–53.
[31] V. Mukherjee, N.P. Singh, R.A. Yadav, Spectrochim. Acta A 73 (2009) 249–256.
[32] T. Sivaranjini, S. Periandy, M. Govindarajan, M. Karabacak, A.M. Asiri, J. Mol. Struct. 1056–1057 (2014) 176–188.
[33] S.K. Pathak, R. Srivastava, A.K. Sachan, O. Prasad, L. Sinha, A.M. Asiri, M. Karabacak, Spectrochim. Acta A 135 (2015) 283–295.
[34] S.K. Pathak, N.G. Haress, A.A. El-Emam, R. Srivastava, O. Prasad, L. Sinha, J. Mol. Struct 1074 (2014) 457–466.
[35] H. Shirani, I. Beigi, Can. J. Chem. 90 (2012) 902–914.
[36] W.C. Huang, P.S. Huang, C.H. Hu, W.B. Tzeng, Chem. Phys. Lett. 580 (2013) 28–31.
[37] D.A. Ellis, Organofluorine Compounds in the Environment-analysis, Sources and Fate, University of Toronto, 2001.
[38] SDBS Web: http://sdbs.riodb.aist.go.jp (National Institute of Advanced Industrial Science and Technology), (2015).
[39] P. Hohenberg, W. Kohn, Phys. Rev. 136 (1964) B864–B871.
[40] A.D. Becke, J. Chem. Phys. 98 (1993) 5648–5652.
[41] A.D. Becke, Phys. Rev. A 38 (1988) 3098–3100.
[42] C. Lee, W. Yang, R.G. Parr, Phys. Rev. B 37 (1988) 785–789.
[43] MJ. Frisch, G.W. Trucks, H.B. Schlegel, G.E. Scuseria, M.A. Robb, J.R. Cheeseman, G. Scalmani, V. Barone, B. Mennucci, G.A. Petersson, et al. Inc., Wallingford, CT (2009).
[44] N.M. O'boyle, A.L. Tenderholt, K.M. Langner, J. Comput. Chem. 29 (2008) 839–845.
[45] T. Lu, F. Chen, J. Comput. Chem. 33 (2012) 580–592.
[46] W. Humphrey, A. Dalke, K. Schulten, J. Mol. Graph 14 (1996) 33–38.
[47] R. Ditchfield, J. Chem. Phys. 56 (1972) 5688–5691.
[48] K. Wolinski, J.F. Hinton, P. Pulay, J. Am. Chem. Soc. 112 (1990) 8251–8260.
[49] M. Karabacak, L. Sinha, O. Prasad, Z. Cinar, M. Cinar, Spectrochim. Acta A 93 (2012) 33–46.
[50] J.B. Foresman, A. Frisch, Gaussian Inc, Pittsburgh, PA (1996) 98–99.
[51] A. Atac, M. Karabacak, C. Karaca, E. Kose, Spectrochim. Acta A 85 (2012) 145–154.
[52] N. Sundaraganesan, S. Ilakiamani, H. Saleem, P.M. Wojciechowski, D. Michalska, Spectrochim. Acta A 61 (2005) 2995–3001.
[53] U. Rani, M. Karabacak, O. Tanrıverdi, M. Kurt, N. Sundaraganesan, Spectrochim. Acta A 92 (2012) 67–77.
[54] M.H. Jamróz, Spectrochim. Acta A 114 (2013) 220–230.
[55] R. Dennington, T. Keith, J. Millam, GaussView, Version 5, 2009.
[56] M. Karabacak, D. Karagöz, M. Kurt, Spectrochim. Acta A 72 (2009) 1076–1083.
[57] M. Karabacak, M. Kurt, M. Çınar, A. Çoruh, Mol. Phys. 107 (2009) 253–264.
[58] M. Karabacak, D. Karagöz, M. Kurt, J. Mol. Struct. 892 (2008) 25–31.
[59] V. Mukherjee, N.P. Singh, R.A. Yadav, Spectrochim. Acta A 73 (2009) 249–256.
[60] P. Wojciechowski, K. Helios, D. Michalska, Vib. Spectrosc. 57 (2011) 126–134.
[61] L. Nygaard, I. Bojesen, T. Pedersen, J. Rastrup-Andersen, J. Mol. Struct. 2 (1968) 209–215.
[62] M. Colapietro, A. Domenicano, C. Marciante, G. Portalone, Acta Crystallogr. Sect. B 37 (1981) 387–394.
[63] M. Karabacak, Z. Cinar, M. Cinar, Spectrochim. Acta A 79 (2011) 1511–1519.
[64] D. Christen, D. Damiani, D.G. Lister, J. Mol. Struct. 41 (1977) 315–317.
[65] I. Altarawneh, K. Altarawneh, A.H. Al-Muhtaseb, S. Alrawadieh, M. Altarawneh, Comput. Theor. Chem. 985 (2012) 30–35.
[66] T. Karthick, V. Balachandran, S. Perumal, A. Nataraj, Spectrochim. Acta A 107 (2013) 72–81.
[67] Z. Zhu, T. Gäumann, Org. Mass Spectrom. 28 (1993) 1111–1118.
[68] M.M. Green, Tetrahedron 36 (1980) 2687–2699.
[69] E. Pretsch, P. Bühlmann, C. Affolter, Structure Determination of Organic Compounds, 2009.
[70] S. Barfuss, K.-H. Emrich, W. Hirschwald, P.A. Dowben, N.M. Boag, J. Organomet. Chem. 391 (1990) 209–218.
[71] W.A. Chupka, J. Chem. Phys. 47 (1967) 2921.
[72] E.L. Chronister, D.M. Szaflarski, M.A. El-Sayed, J. Silberstein, I. Salman, R.D. Levine, J. Phys. Chem. 92 (1988) 2824–2827.
[73] D. Guillaumont, S. Nakamura, Dye. Pigment. 46 (2000) 85–92.
[74] J. Fabian, Dye. Pigment. 84 (2010) 36–53.
[75] M. Karabacak, E. Kose, A. Atac, A.M. Asiri, M. Kurt, J. Mol. Struct. 1058 (2014) 79–96.
[76] M. Arivazhagan, D. Anitha Rexalin, Spectrochim. Acta A 96 (2012) 668–676.
[77] V. Balachandran, A. Nataraj, T. Karthick, M. Karabacak, A. Atac, J. Mol. Struct. 1027 (2012) 1–14.
[78] R.G. Parr, R.G. Pearson, J. Am. Chem. Soc. 105 (1983) 7512–7516.
[79] R.G. Parr, W. Yang, Density-functional Theory of Atoms and Molecules, Oxford University Press, USA, 1989.
[80] R. Hoffman, Solids and Surfaces: a Chemist's View of Bonding in Extended Structures, 1988.
[81] T. Hughbanks, R. Hoffmann, J. Am. Chem. Soc. 105 (1983) 3528–3537.
[82] J.G. Małecki, Polyhedron 29 (2010) 1973–1979.
[83] S.I. Gorelsky, S. Ghosh, E.I. Solomon, J. Am. Chem. Soc. 128 (2005) 278–290.
[84] S. Ghosh, S.I. Gorelsky, P. Chen, I. Cabrito, J.J.G. Moura, I. Moura, E.I. Solomon,

J. Am. Chem. Soc. 125 (2003) 15708–15709.
[85] C. Platas-Iglesias, D. Esteban-Gómez, T. Enríquez-Pérez, F. Avecilla, A. de Blas, T. Rodríguez-Blas, Inorg. Chem. 44 (2005) 2224–2233.
[86] M. Chen, U.V. Waghmare, C.M. Friend, E. Kaxiras, J. Chem. Phys. 109 (1998) 6854–6860.
[87] E. Kose, A. Atac, M. Karabacak, C. Karaca, M. Eskici, A. Karanfil, Spectrochim. Acta A 97 (2012) 435–448.
[88] N. Okulik, A.H. Jubert, Internet Electron. J. Mol. Des. 4 (2005) 17–30.
[89] F.J. Luque, J.M. López, M. Orozco, Theor. Chem. Accounts Theory, Comput. Model. Theoretica Chim. Acta 103 (2000) 343–345.
[90] M. Govindarajan, M. Karabacak, Spectrochim. Acta A. 96 (2012) 421–435.
[91] R.S. Mulliken, J. Chem. Phys. 23 (1955) 1833–1840.
[92] E.R. Johnson, S. Keinan, P. Mori-Sánchez, J. Contreras-García, A.J. Cohen, W. Yang, (2010) 6498–6506.
[93] T. Schlick, Molecular Modeling and Simulation: an Interdisciplinary Guide: an Interdisciplinary Guide, second ed., Springer, Newyork, USA, 2010.
[94] M. Karabacak, M. Cinar, M. Kurt, J. Mol. Struct. 968 (2010) 108–114.
[95] N. Subramanian, N. Sundaraganesan, J. Jayabharathi, Spectrochim. Acta A 76 (2010) 259–269.
[96] M. Karabacak, C. Karaca, A. Atac, M. Eskici, A. Karanfil, E. Kose, Spectrochim. Acta A 97 (2012) 556–567.
[97] H.O. Kalinowski, S. Berger, S. Braun, Carbon-13 NMR Spectroscopy, 1988.
[98] K. Pihlaja, E. Kleinpeter, Carbon-13 NMR Chemical Shifts in Structural and Stereochemical Analysis, VCH, 1994.
[99] S. Ramalingam, M. Karabacak, S. Periandy, N. Puviarasan, D. Tanuja, Spectrochim. Acta A 96 (2012) 207–220.
[100] M. Karabacak, E. Kose, A. Atac, M. Ali Cipiloglu, M. Kurt, Spectrochim. Acta A 97 (2010) 892–908.
[101] A. Altun, K. Gölcük, M. Kumru, J. Mol. Struct. Theochem 625 (2003) 17–24.
[102] R.M. Silverstein, G.C. Bassler, T.C. Morrill, Spectrometric Identification of Organic Compounds, Wiley, 1981.
[103] A. Altun, K. Gölcük, M. Kumru, J. Mol. Struct. Theochem 637 (2003) 155–169.
[104] M. Govindarajan, M. Karabacak, S. Periandy, D. Tanuja, Spectrochim. Acta A 97 (2012) 231–245.
[105] N. Sundaraganesan, J. Karpagam, S. Sebastian, J.P. Cornard, Spectrochim. Acta A 73 (2009) 11–19.
[106] A. Altun, K. Gölcük, M. Kumru, Vib. Spectrosc. 31 (2003) 215–225.
[107] A. Altun, K. Gölcük, M. Kumru, Vib. Spectrosc. 33 (2003) 63–74.
[108] S. Singh, N. Singh, Indıan J. Pure Applıed Physıcs 7 (1969) 250–252.
[109] P. Wojciechowski, J. Fluor. Chem. 154 (2013) 7–15.
[110] E. Kose, M. Karabacak, A. Atac, J. Mol. Struct. Spectrochim. Acta A 143 (2015) 265–280.
[111] G. Varsányi, Assignments for Vibrational Spectra of Seven Hundred Benzene Derivatives, Halsted Press, 1974.
[112] R.M. Silverstein, F.X. Webster, D.J. Kiemle, Spectrometric Identification of Organic Compounds, John Wiley & Sons, 2005.
[113] H.M. Badawi, W. Förner, S.A. Ali, Spectrochim. Acta A 112 (2013) 388–396.